

# Anomalous magnetic and weak magnetic dipole moments of the $\tau$ lepton in the simplest little Higgs model

M. A. Arroyo-Ureña, G. Hernández-Tomé, and G. Tavares-Velasco

*Facultad de Ciencias Físico-Matemáticas  
Benemérita Universidad Autónoma de Puebla,  
C.P. 72570, Puebla, Pue., Mexico*

(Dated: January 10, 2017)

We obtain analytical expressions, both in terms of parametric integrals and Passarino-Veltman scalar functions, for the one-loop contributions to the anomalous weak magnetic dipole moment (AWMDM) of a charged lepton in the framework of the simplest little Higgs model (SLHM), which predicts new particles and corrections to the couplings of the standard model (SM). Such results are very general and can be useful to compute the weak properties of a charged lepton in other extension models. As a by-product we obtain the corresponding contributions to the anomalous magnetic dipole moment (AMDM), which agree with previous results. We then study numerically the potential contributions from this model to the tau lepton AMDM and AWMDM for values of the parameter space consistent with current experimental data. It is found that they depend mainly on the energy scale  $f$  at which the global symmetry is broken and the  $t_\beta$  parameter, whereas there is little sensitivity to a mild change in the values of other parameters of the model. While the tau AMDM is of the order of  $10^{-9}$ , the real (imaginary) part of its AWMDM is of the order of  $10^{-9}$  ( $10^{-10}$ ). A comparison of the SLHM predictions and those of other SM extensions is done.

## I. INTRODUCTION

The most general dimension-five effective interaction of a neutral  $V$  gauge boson ( $V = \gamma, Z$ ) to a charged lepton that respects Lorentz invariance can be written in terms of six independent form factors:

$$\Gamma_\mu^{\ell\ell V}(q^2) = ie \left[ \gamma_\mu (F_V^V - F_V^V \gamma_5) - q_\mu (iF_S^V + F_P^V \gamma_5) + \sigma_{\mu\nu} q^\nu (iF_M^V + F_E^V \gamma_5) \right], \quad (1)$$

where  $q$  is the incoming transfer four-momentum of the gauge boson. The electromagnetic (weak) properties of the lepton are determined by the photon ( $Z$  gauge boson) vertex function. The  $CP$ -violating terms define the static electric dipole moment (EDM) and the static weak electric dipole moment (WEDM):

$$d_\ell = -eF_E^\gamma(0), \quad (2)$$

$$d_\ell^W = -eF_E^Z(m_Z^2). \quad (3)$$

Since the standard model (SM) predictions for these  $CP$ -violating dipole moments are highly suppressed, they may serve to search for new sources of  $CP$  violation. In this work we are interested instead in the static anomalous magnetic dipole moment (AMDM) and the static anomalous weak magnetic dipole moment (AWMDM), which are defined in terms of the  $CP$ -even form factor as follows:

$$a_\ell = -2m_\ell F_M^\gamma(0), \quad (4)$$

$$a_\ell^W = -2m_\ell F_M^Z(m_Z^2). \quad (5)$$

The measurement of the AMDM of a lepton has long been considered a probe for the SM, which considers leptons as point-like objects. The AMDM of the electron  $a_e$ , which receives its main contributions from quantum electrodynamics (QED), has been calculated up to order of  $\alpha^5$  [1] and the agreement between the theoretical and the experimental values has reached the level of ten significant digits [2], which represents one of the greatest milestones of QED.

As far as the muon is concerned, the E821 experiment at Brookhaven National Lab (BNL) measured its AMDM  $a_\mu$  with an unprecedented precision of 0.54 ppm. The current average experimental measurement is  $a_\mu^{Exp.} = 11659209.1(5.4)(3.3) \times 10^{-10}$  [3], and further improvement is expected in future experiments by the  $(g-2)_\mu$  [4] and J-PARC  $(g-2)$ /EDM [5] Collaborations, which aim to reach a precision of  $\pm 0.2$  ppm. As for the theoretical prediction of the SM,  $a_\mu^{SM} = 116591803(1)(42)(26) \times 10^{-11}$  [6], there is still a large uncertainty in the estimate of the hadronic contribution, whereas the QED and electroweak contributions have been determined with a great precision [7]. Thus a more accurate evaluation of the leading order hadronic contribution together with the future experimental

measurement are needed to settle down the discrepancy between the SM prediction and the experimental value of  $a_\mu$ , which currently stands at the level of 3.6 standard deviations [6]:

$$\Delta a_\mu = a_\mu^{Exp.} - a_\mu^{SM} = 288(63)(49) \times 10^{-11}. \quad (6)$$

Since the muon AMDM has become a powerful tool to test the validity of the SM and searching for new physics (NP) effects, a plethora of calculations within the framework of several SM extensions has been reported in the literature in order to explain the  $\Delta a_\mu$  discrepancy [8].

As far as the  $\tau$  lepton is concerned, its short lifetime ( $290.3 \pm 0.5 \times 10^{-15}$  s) [9] does not allow for a measurement of its AMDM with a high precision by a spin precession method. The most stringent current bound on  $a_\tau$  is [10]

$$-0.052 < a_\tau < 0.013, \quad (7)$$

which was obtained using LEP1, SLD and LEP2 data for tau lepton production. It also has been pointed out recently that the tau electromagnetic moments can be probed in  $\gamma\gamma$  and  $\gamma e$  collisions at CLIC, which can lead to improved bounds [11, 12]. Although the existing bounds are far from the SM prediction  $a_\tau^{SM} = 117721(5) \times 10^{-8}$  [13, 14], a more precise determination of the experimental value is required before any conclusion is drawn. In this regard, it has been pointed out that super  $B$  factories could allow for a precise determination of  $a_\tau$  up to the  $10^{-6}$  level using unpolarized or polarized electron beams [15–17]. Furthermore, due to its large mass, it is expected that the tau AMDM can be very sensitivity to NP effects [18] since its electroweak contribution would be ten times larger than the uncertainty of the hadronic contribution [14]. Therefore, it is worth estimating the tau AMDM in any SM extension as future measurements may allow us to search for NP in a rather clean environment.

Unlike the electromagnetic dipole moments of leptons, little attention has been paid to the study of their weak properties. In the experimental arena, the current best limits on the tau AWMDM and WEDM, with 95% C.L., are [19]

$$Re(a_\tau^W) < 1.14 \times 10^{-3}, \quad (8)$$

$$Im(a_\tau^W) < 2.65 \times 10^{-3}, \quad (9)$$

$$Re(d_\tau^W) < 0.5 \times 10^{-17} \text{ ecm}, \quad (10)$$

$$Im(d_\tau^W) < 1.1 \times 10^{-17} \text{ ecm}, \quad (11)$$

which were extracted from the data collected at the LEP from 1990 to 1995, corresponding to an integrated luminosity of  $155 \text{ pb}^{-1}$ . Somewhat weaker bounds were obtained in [20] via a study of the  $pp \rightarrow \tau^+\tau^-$  and  $pp \rightarrow Zh \rightarrow \tau^+\tau^-h$  cross sections at the LHC. The experimental bounds on  $a_\tau^W$  is far above from the SM theoretical prediction [21]:

$$a_\tau^W = -(2.10 + 0.61i) \times 10^{-6}, \quad (12)$$

which leaves enough room to potentially large contributions from NP.

In this work we will evaluate the AMDM and AWMDM of a lepton, with special focus on those of the tau lepton, predicted by the simplest little Higgs model (SLHM) [22], which is an appealing SM extension. This model is aimed to deal with the hierarchy problem by conjecturing that the Higgs boson is a pseudo-Goldstone boson arising from a global symmetry broken spontaneously. At the same scale, the local symmetry is also broken by a collective symmetry breaking mechanism. The top quark and the electroweak gauge bosons have heavy partners that give rise to new contributions that exactly cancel the quadratic divergences to the Higgs boson mass at the one-loop level, thereby rendering a mass of about one hundred GeV without the need of fine tuning [23, 24].

The rest of this presentation is organized as follows. A brief review on the SLHM is presented in the Section II, whereas Sec. III is devoted to the analytical results for the AWMDM. As a byproduct we will obtain the corresponding expressions for the AMDM. The numerical behavior of the tau electromagnetic and weak dipole moments is analyzed in Section IV, and the conclusion and outlook are presented in Section V. The Feynman rules and the explicit expressions for the loop integrals are presented in the appendices.

## II. THE SIMPLEST LITTLE HIGGS MODEL

We now present an overview of the SLHM focusing only on the details relevant for our calculation. For a detailed account of this model and the study of its phenomenology we refer the reader to Refs. [22, 25–28], which we will follow closely in our discussion below. The SLHM is the most economic version of simple-group little Higgs models, which have the feature that the SM gauge group is embedded into a larger simple gauge group instead of a product

gauge group. The SLHM has a global symmetry under the  $[SU(3) \times U(1)]^2$  group and a gauge symmetry under the diagonal subgroup  $SU(3)_L \times U(1)_X$ , which requires the introduction of nine gauge bosons. At the TeV scale, the global symmetry is broken down spontaneously to  $[SU(2) \times U(1)]^2$  via the vacuum expectation values (VEVs)  $f_1$  and  $f_2$  of two sigma fields  $\Phi_1$  and  $\Phi_2$ , giving rise to ten Goldstone bosons. At the same scale the gauge group breaks to the SM gauge group  $SU(2)_L \times U(1)_Y$  and five Goldstone bosons are eaten by the heavy fields: a charged gauge boson  $X^\pm$ , a no-self conjugate neutral boson  $Y_0 \neq Y_0^\dagger$ , and an extra neutral gauge boson  $Z'$ , which thus acquire masses of the order of the scale  $f_1 \sim f_2$ . The remaining Goldstone bosons are accommodated in a complex doublet (the SM one) and a real singlet of  $SU(2)$ . The Goldstone bosons can be parametrized by the triplets

$$\Phi_1 = e^{i\Theta \frac{f_2}{f_1}} \begin{pmatrix} 0 \\ 0 \\ f_1 \end{pmatrix}, \quad \Phi_2 = e^{-i\Theta \frac{f_1}{f_2}} \begin{pmatrix} 0 \\ 0 \\ f_2 \end{pmatrix}, \quad (13)$$

where the pion matrix is

$$\Theta = \frac{1}{f} \begin{pmatrix} \frac{\eta}{\sqrt{2}} & 0 & h \\ 0 & \frac{\eta}{\sqrt{2}} & h^\dagger \\ h^\dagger & h^\dagger & \frac{\eta}{\sqrt{2}} \end{pmatrix}, \quad (14)$$

here  $f = \sqrt{f_1^2 + f_2^2}$ ,  $h$  is the  $SU(2)$  complex doublet of the SM, and  $\eta$  is the real scalar field. The normalization is chosen to produce canonical kinetic terms. The dynamics of the Goldstone bosons is described by a non-linear sigma model

$$\mathcal{L}_{kin} = |D_\mu \Phi_1|^2 + |D_\mu \Phi_2|^2, \quad (15)$$

with the  $SU(3)_L \times U(1)_X$  covariant derivative

$$D_\mu = \partial_\mu + igT^a A_\mu^a - ig_X Q_X B_\mu^X, \quad (16)$$

where  $T^a$  ( $a = 1 \dots 8$ ) are the  $SU(3)_L$  generators in the fundamental representation,  $A_\mu^a$  are the  $SU(3)_L$  gauge fields,  $B_\mu^X$  is the  $U(1)_X$  gauge field, and  $Q_X = -1/3$  for  $\Phi_1$  and  $\Phi_2$ . The new gauge bosons accommodate in a complex  $SU(2) \times U(1)$  doublet ( $X^\pm, Y_0$ ) with hypercharge  $\frac{1}{2}$  and a neutral singlet  $Z'_0$ . The matching of the gauge coupling constants yields

$$g_X = \frac{gt_W}{\sqrt{1 - t_W^2/3}}, \quad (17)$$

with  $t_W = s_W/c_W$  the tangent of the Weinberg angle  $\theta_W$ .

As mentioned above, after the first stage of symmetry breaking, there emerge the pair of charged gauge bosons  $X^\pm$ , the no-self conjugate neutral gauge boson  $Y_0$ , and the neutral gauge boson  $Z'_0$  (following Ref. [25] we will denote the gauge eigenstates with the subindex 0)

$$X^\pm = \frac{1}{\sqrt{2}}(A^6 \mp iA^7), \quad (18)$$

$$Y_0 = \frac{1}{\sqrt{2}}(A^4 - iA^5), \quad (19)$$

$$Z'_0 = \frac{1}{\sqrt{3}} \left( \sqrt{3 - t_W^2} A^8 + t_W B^X \right), \quad (20)$$

with masses of the order of  $f$ . Four gauge fields remain massless at this stage. While  $A^1, A^2, A^3$  identify with the  $SU(2)_L$  gauge bosons  $W^a$ , the charged gauge bosons  $W^\pm$  and the hypercharge gauge boson are

$$W^\pm = \frac{1}{\sqrt{2}}(A^1 \mp iA^2), \quad (21)$$

$$B = -\frac{1}{3} \left( t_W A^8 + \sqrt{3 - t_W^2} B^X \right). \quad (22)$$

After the electroweak symmetry breaking (EWSB), the weak gauge bosons  $W^\pm$  and  $Z_0$  acquire mass and the heavy gauge boson masses get corrected. Up to order  $(v/f)^2$   $W, X$  and  $Y_0$  coincide with the mass eigenstates and their masses are [26]

$$m_W = \frac{gv}{2} \left( 1 - \frac{v^2}{12f^2} \left( \frac{s_\beta^4}{c_\beta^2} + \frac{c_\beta^4}{s_\beta^2} \right) \right), \quad (23)$$

$$m_X = \frac{gf}{\sqrt{2}} \left( 1 - \frac{v^2}{4f^2} \right), \quad (24)$$

$$m_Y = \frac{gf}{\sqrt{2}}, \quad (25)$$

with  $t_\beta = \tan \beta = f_1/f_2$ . If higher order terms are considered  $W$  and  $X$  need to be rotated to obtain the physical states [26]. On the other hand, the photon and the light neutral  $Z_0$  gauge boson are given by

$$A = s_W A^3 + c_W B, \quad (26)$$

$$Z_0 = c_W A^3 - s_W B. \quad (27)$$

Finally,  $Z_0$  and  $Z'_0$  need to be rotated to obtain the mass eigenstates, which we call  $Z$  and  $Z'$  given by

$$Z'_0 = Z' + \delta_Z Z, \quad (28)$$

$$Z_0 = Z - \delta_Z Z', \quad (29)$$

with  $\delta_Z = -\frac{(1-t_W^2)\sqrt{3-t_W^2}}{8c_W} \frac{v^2}{f^2}$ . The respective masses, up to order  $(v/f)^2$ , are [26]

$$m_Z = \frac{gv}{2c_W} \left( 1 - \frac{v^2}{12f^2} \left( \frac{s_\beta^4}{c_\beta^2} + \frac{c_\beta^4}{s_\beta^2} \right) - \frac{v^2}{16f^2} (1-t_W^2)^2 \right), \quad (30)$$

$$m_{Z'} = \frac{\sqrt{2}gf}{\sqrt{3-t_W^2}} \left( 1 - \frac{v^2}{f^2} \frac{(3-t_W^2)}{16c_W^2} \right). \quad (31)$$

The kinetic Lagrangian of the gauge bosons gives rise to the trilinear gauge boson couplings necessary for our calculation. It can be written as

$$\mathcal{L}^G = -\frac{1}{4} B^{X\mu\nu} B_{\mu\nu}^X - \frac{1}{4} A^{a\mu\nu} A_{\mu\nu}^a, \quad (32)$$

with the Abelian and non-Abelian gauge strength tensors

$$B_{\mu\nu}^X = \partial_\mu B_\nu^X - \partial_\nu B_\mu^X, \quad (33)$$

and

$$A_{\mu\nu}^a = \partial_\mu A_\nu^a - \partial_\nu A_\mu^a + gf_{abc} A_\mu^b A_\nu^c, \quad (34)$$

with  $f_{abc}$  the structure constants of the  $SU(3)$  group. From the relations between gauge eigenstates and mass eigenstates (18)-(22) and (26)-(29) we can obtain after some lengthy algebra the Feynman rules listed in Appendix A for the  $VV_j^\pm V_j^\mp$  vertices, namely  $AW^\pm W^\mp$ ,  $AX^\pm X^\mp$ ,  $ZW^\pm W^\mp$ , and  $ZX^\pm X^\mp$ .

In the lepton sector of the SLHM, for each generation there is a left-handed triplet  $L_m^T = (\nu_{Lm}, \ell_{Lm}, iN_{Lm})$ , which is completed with a new neutral lepton  $N_{Lm}$ , and two right-handed singlets  $\ell_{Rm}$  and  $N_{Rm}$ . The Yukawa Lagrangian can be written, in the basis where flavor and mass  $N_m$  eigenstates coincide, as

$$\mathcal{L}_Y = i\lambda_N^m \bar{N}_{Rm} \Phi_2^\dagger L_m + \frac{i\lambda_\ell^{mn}}{\Lambda} \bar{\ell}_{Rm} \epsilon_{ijk} \Phi_1^i \Phi_2^j L_n^k + \text{H.c.}, \quad (35)$$

where  $\Lambda = 4\pi f$  is the cutoff of the effective theory. Here  $m$  and  $n$  are generation indices, whereas  $i, j$ , and  $k$  are  $SU(3)$  indices. After EWSB this Lagrangian yields the lepton masses and the heavy neutrino masses up to order  $(v/f)^2$  [26]

$$\begin{aligned} \mathcal{L}_{mass} = & -fs_\beta \lambda_N^m \left( \left( 1 - \frac{\delta_\nu^2}{2} \right) \bar{N}_{Rm} N_{Lm} - \delta_\nu \bar{N}_{Rm} \nu_{Lm} \right) \\ & + \left( 1 - \frac{v^2}{4f^2} - \frac{v^2}{41f^2} \left( \frac{s_\beta^4}{c_\beta^2} + \frac{c_\beta^4}{s_\beta^2} \right) \right) \frac{fv}{\sqrt{2}\Lambda} \lambda_\ell^{mn} \bar{\ell}_{Rm} \ell_{Ln} + \text{H.c.}, \end{aligned} \quad (36)$$

where  $\delta_\nu = \frac{v}{\sqrt{2}ft_\beta}$  represents the mixing between a heavy neutrino and a SM neutrino of the same generation. Notice also that the rotation that diagonalizes  $\lambda_N$  does not necessarily diagonalizes  $\lambda_\ell$  so there is mixing between the charged leptons and the heavy neutrinos mediated by the charged gauge bosons. The charged lepton mass eigenstates  $\ell_{Lm}$  are thus related to the flavor eigenstates  $\ell_{Lm0}$  by the rotation

$$\ell_{Lm0} = V^{mi} \ell_{Li}. \quad (37)$$

where  $V^{mi}$  is a CKM-like mixing matrix. Also, in each generation, the SM and heavy neutrino mass eigenstates are obtained through

$$\nu_{Li0} = \left(1 - \frac{\delta_\nu^2}{2}\right) \nu_{Li} - \delta_\nu V^{im} N_{Lm}, \quad (38)$$

$$N_{Lm0} = \left(1 - \frac{\delta_\nu^2}{2}\right) N_{Lm} + \delta_\nu V^{mi} \nu_{Li}, \quad (39)$$

where again the 0 subindex stands for flavor eigenstates. The lepton masses up to order  $(v/f)^2$  are [26]

$$m_\ell = - \left(1 - \frac{v^2}{4f^2} - \frac{v^2}{41f^2} \left(\frac{s_\beta^4}{c_\beta^2} + \frac{c_\beta^4}{s_\beta^2}\right)\right) \frac{fv}{\sqrt{2}\Lambda} y_\ell, \quad (40)$$

where  $y_\ell$  is the eigenvalue of the  $\lambda_\ell$  matrix and

$$m_{N_i} = f s_\beta \lambda_N^i. \quad (41)$$

The vertices of a gauge boson to a lepton pair are obtained from the lepton kinetic Lagrangian, which can be written as

$$\mathcal{L}_F = \bar{L}_m i \gamma^\mu D_\mu L_m + \bar{\ell}_{Rm} i \gamma^\mu D_\mu \ell_{Rm} + \bar{N}_{Rm} i \gamma^\mu N_{Rm}, \quad (42)$$

where the covariant derivative was given in Eq. (16), with  $Q_X = -1/3, 0$  and  $1$  for  $L_m, N_m$  and  $\ell_m$ . We need to introduce the mass eigenstates to obtain the interactions of the physical gauge bosons  $Z, W, X$ , and  $Z'$  to a lepton pair, which are necessary for our calculation of the AMDM and AWMDM of a lepton. They are given by

$$\begin{aligned} \mathcal{L}_{Zff'} = & -\frac{g}{c_W} Z_\mu \left[ \left(-\frac{1}{2} + s_W^2\right) \bar{\ell}_{Li} \gamma^\mu \ell_{Li} + \frac{1}{2} (1 - \delta_\nu^2) \bar{\nu}_{Li} \gamma^\mu \nu_{Li} + s_W^2 \bar{\ell}_{Ri} \gamma^\mu \ell_{Ri} \right. \\ & + \frac{1}{2} \delta_\nu^2 \bar{N}_{Li} \gamma^\mu N_{Li} - \frac{1}{2} (\delta_\nu V^{im} \bar{N}_{Lm} \gamma^\mu \nu_{Li} + \text{H.c.}) \\ & \left. + \frac{\delta_Z}{c_W \sqrt{3 - t_W^2}} \left( \left(\frac{1}{2} - s_W^2\right) (\bar{\ell}_{Li} \gamma^\mu \ell_{Li} + \bar{\nu}_{Li} \gamma^\mu \nu_{Li}) - s_W^2 \bar{\ell}_{Ri} \gamma^\mu \ell_{Ri} - c_W^2 \bar{N}_{Li} \gamma^\mu N_{Li} \right) \right], \end{aligned} \quad (43)$$

$$\mathcal{L}_{Wff'} = -\frac{g}{\sqrt{2}} W_\mu^- \left( \left(1 - \frac{\delta_\nu^2}{2}\right) \bar{\ell}_{Li} \gamma^\mu \nu_{Li} - \frac{1}{2} \delta_\nu V^{im} \bar{\ell}_{Li} \gamma^\mu N_{Lm} \right) + \text{H.c.}, \quad (44)$$

$$\mathcal{L}_{Xff'} = -i \frac{g}{\sqrt{2}} X_\mu^- \left( \delta_\nu \bar{\ell}_{Li} \gamma^\mu \nu_{Li} + \left(1 - \frac{\delta_\nu^2}{2}\right) \bar{\ell}_{Li} \gamma^\mu V^{im} N_{Lm} \right) + \text{H.c.}, \quad (45)$$

and

$$\begin{aligned} \mathcal{L}_{Z\ell\ell} = & \frac{g}{c_W \sqrt{3 - t_W^2}} Z'_\mu \left[ \left(-\frac{1}{2} + s_W^2\right) \bar{\ell}_{Li} \gamma^\mu \ell_{Li} + s_W^2 \bar{\ell}_{Ri} \gamma^\mu \ell_{Ri} \right. \\ & \left. + \delta_Z c_W \sqrt{3 - t_W^2} \left( \left(-\frac{1}{2} + s_W^2\right) \bar{\ell}_{Li} \gamma^\mu \ell_{Li} + s_W^2 \bar{\ell}_{Ri} \gamma^\mu \ell_{Ri} \right) \right]. \end{aligned} \quad (46)$$

Notice that there is lepton flavor violation mediated by the charged gauge bosons. Finally, the interactions of the photon with a charged lepton pair are dictated by QED

$$\mathcal{L}_{A\ell\ell} = -eA_\mu \bar{\ell} \gamma^\mu \ell. \quad (47)$$

There are also contributions to the AMDM and the AWMDM of a lepton from the scalar Higgs bosons  $H$  and  $\eta$ . From the Lagrangian (15) we can obtain the respective interactions with the  $Z$  and  $Z'$  gauge bosons. After some algebra one can extract the vertices  $ZZ'H$  and  $ZZH$ , which are given as follows to the leading order in  $(v/f)$  as

$$\mathcal{L}_{ZZ'H} = \frac{g^2 v (1 - t_W^2)}{2c_W \sqrt{3 - t_W^2}} H Z^\mu Z'_\mu, \quad (48)$$

together with the usual SM interaction

$$\mathcal{L}_{ZZH} = g m_Z H Z^\mu Z'_\mu, \quad (49)$$

From the Yukawa Lagrangian (35) we can also obtain the interactions of the scalar Higgs bosons  $H$  and  $\eta$  to leptons, which we need for our calculation. They are diagonal and are given to leading order in  $(v/f)^2$  by [25]

$$\mathcal{L}_{H\bar{\ell}\ell} = ig \frac{m_\ell}{2m_W} \left( 1 - \frac{v^2}{6f^2} \left( \frac{1}{t_\beta} + t_\beta \right)^2 \right) \bar{\ell} \ell H, \quad (50)$$

and

$$\mathcal{L}_{\eta\bar{\ell}\ell} = ig \frac{m_\ell}{\sqrt{2}f} \left( \frac{1}{t_\beta} - t_\beta \right) \bar{\ell} \gamma^5 \ell \eta. \quad (51)$$

The  $\eta ZZ'$  vertex vanish since  $\eta$  is  $CP$ -odd scalar, but the  $H\eta Z$  coupling does arise, though its contribution to the AMDM and AWMDM of a lepton vanishes. Other details of this model are irrelevant for our calculation so we refrain from presenting a discussion of the quark sector and the Coleman-Weinberg scalar potential.

### III. ANOMALOUS MAGNETIC AND WEAK MAGNETIC DIPOLE MOMENTS IN THE SLHM

We now turn to present the analytical expressions for the AMDM and AWMDM of a lepton within the SLHM. Since there is no  $CP$ -violation in this model, both the EDM and the WEDM vanish. All the Feynman rules necessary for our calculation follow straightforwardly from the above interaction lagrangians and are presented in Appendix A. Since all the particles are on their mass shell, the loop amplitudes are gauge independent. We used the unitary gauge as it is best suited for our calculation method. In order to solve the loop integrals, we used both Feynman parametrization and the Passarino-Veltman reduction scheme. We will first present the results for the AWMDM, from which the results for the AMDM will follow easily.

#### A. Anomalous weak magnetic dipole moment

In the SLHM, in addition to the pure SM contributions, the AWMDM receives new physics contributions arising from the loops carrying only new particles, but also from loops involving only SM particles. The latter are due to corrections to the SM vertices and appear as a series of powers of  $v/f$ , so it is enough to consider the leading order terms. The AWMDM of lepton  $\ell_i$  can thus be written as

$$a_{\ell_i}^{W-SLHM} = a_{\ell_i}^{W-SM} + a_{\ell_i}^{W-NP}, \quad (52)$$

where  $a_{\ell_i}^{W-SM}$  stands for the pure SM contributions and  $a_{\ell_i}^{W-NP}$  stands for the new physics contributions, which can be written as

$$a_{\ell_i}^{W-NP} = a_{\ell_i}^{W-Gauge} + a_{\ell_i}^{W-Scalar}, \quad (53)$$

with  $a_{\ell_i}^{W-Gauge}$  ( $a_{\ell_i}^{W-Scalar}$ ) the contributions arising from the gauge (scalar) sector of the SLHM.

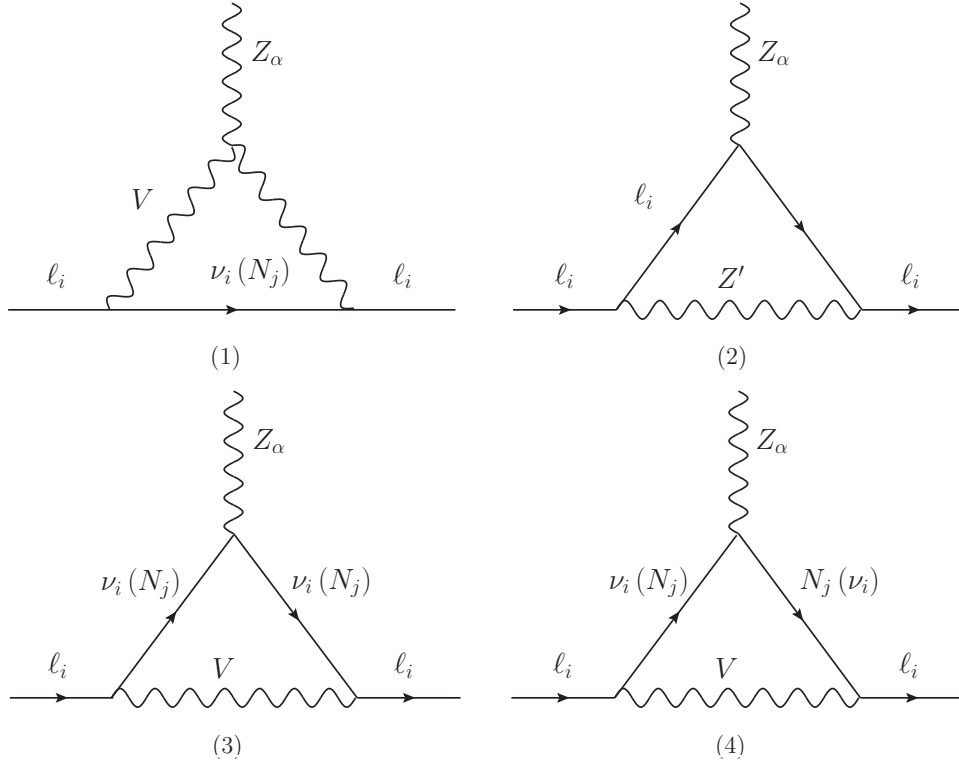


FIG. 1: Feynman diagrams that contribute to the the AWMDM of charged lepton  $\ell_i$  at the one-loop level in the gauge sector of the SLHM. Here  $V$  can be either the  $W$  gauge boson or the new charged  $X$  gauge boson,  $\nu_i$  and  $N_j$  stand for a SM neutrino and a new heavy one predicted by the SLHM, respectively. Notice that diagram (3) involves the vertex  $Z\bar{\nu}_i N_j$ .

In the gauge sector, the NP contributions to the AWMDM arise from the Feynman diagrams of Fig. 1, where  $V$  stands for the charged gauge bosons  $W$  and  $X$ ,  $\nu_i$  is a SM neutrino, and  $N_i$  is a heavy neutrino. According to our discussion above, for the loops involving only  $W$  gauge bosons and SM neutrinos we consider the leading order  $v/f$  contributions arising from the corrections to the  $W\ell\nu$  vertex. The contributions to the AWMDM of each Feynman diagram will be written as follows

$$a_{\ell_i}^{W-A_1 A_2 A_3} = \frac{\alpha}{4\pi} f_Z^{A_1 A_2 A_3} I_Z^{A_1 A_2 A_3} \quad (54)$$

where the three-letter superscript stands for the particles circulating into each loop diagram ( $A_2$  and  $A_3$  are the particles attached to the external  $Z$  gauge boson, whereas  $A_1$  is the particle attached to the external leptons). Here  $f_Z^{A_1 A_2 A_3}$  are coefficients involving all the couplings appearing in each amplitude, whereas  $I_Z^{A_1 A_2 A_3}$  stand for the loop integrals, which depend on the masses of the virtual particles. We present in Appendix B both the  $f_Z^{A_1 A_2 A_3}$  coefficients and the loop integrals in terms of parametric integrals and Passarino-Veltman scalar functions. We have verified that the contribution of each diagram to the AWMDM is free of ultraviolet divergences. The full contribution of the gauge sector can be written as

$$a_{\ell_i}^{W-Gauge} = \sum_{V=W,X} \sum_{n=\nu_i, N_j} (a_{\ell_i}^{W-nVV} + a_{\ell_i}^{W-Vnn}) + a_{\ell_i}^{W-Z'\ell_i\ell_i}, \quad (55)$$

where the index  $j$  runs over the three lepton families.

In the scalar sector of the SLHM there are contributions to the AWMDM of a lepton arising from both the SM scalar boson  $H$  and the new pseudoscalar boson  $\eta$  via the Feynman diagrams of Fig. 2. The contributions of the SM Higgs boson arise from corrections of the order of  $(v/f)^2$  to the SM vertices  $H\ell\ell$  and  $HZZ$ . The respective contributions to the AWMDM can also be written as in Eq. (54), where the  $f_Z^{A_1 A_2 A_3}$  coefficients and the  $I_Z^{A_1 A_2 A_3}$  functions are presented in Appendix B. Again we have verified that the contribution of each diagram to the AWMDM is ultraviolet finite.

The full scalar contribution is thus

$$a_{\ell_i}^{W-Scalar} = \sum_{S=\eta, H} a_{\ell_i}^{W-S\ell_i\ell_i} + \sum_{V=Z, Z'} a_{\ell_i}^{W-\ell_i HV}. \quad (56)$$

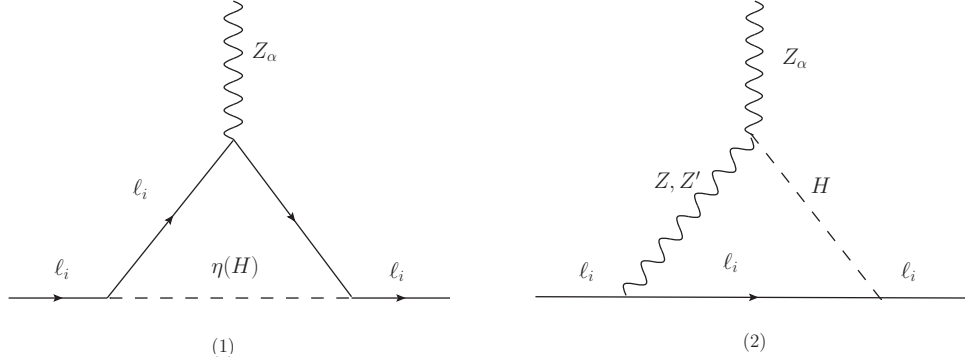


FIG. 2: Feynman diagrams that contribute to the AWMDM of a lepton in the scalar sector of the SLHM at the one-loop level. We do not show the diagram obtained by exchanging the  $Z(Z')$  gauge boson and the Higgs boson in diagram (2). The new contributions of the SM Higgs boson contributions are due to the diagram with the  $Z'$  gauge boson and also to corrections to the SM vertices  $H\ell\ell$  and  $HZZ$ .

### B. Anomalous magnetic dipole moment

In the gauge sector of the SLHM, the AMDM of a lepton arises from the Feynman diagrams (1) and (2) of Fig. 1, with the  $Z$  gauge boson replaced by the photon. There are also contributions arising from the scalar sector, which are induced by the scalar bosons  $H$  and  $\eta$  via a Feynman diagram similar to diagram (1) of Fig. 2. The corresponding contributions to the AMDM can be obtained straightforwardly from those to the AWMDM by considering the limit  $m_Z \rightarrow 0$  and substituting the  $Z$  coupling constants by those of the photon. We can write the contributions to  $a_\ell$  arising from each diagram as

$$a_{\ell_i}^{A_1 A_2 A_3} = \frac{\alpha f_\gamma^{A_1 A_2 A_3}}{4\pi} I_\gamma^{A_1 A_2 A_3}, \quad (57)$$

where again the three-letter superscript corresponds to the three particles circulating into the loop. Explicit expressions for the  $f_\gamma^{A_1 A_2 A_3}$  constants and the  $I_\gamma^{A_1 A_2 A_3}$  functions are presented in Appendix B.

The overall NP contribution of the SLHM to  $a_{\ell_i}$  is thus

$$a_{\ell_i}^{NP} = \sum_{V=W, X} \sum_{n=\nu_i, N_j} a_{\ell_i}^{nVV} + a_\ell^{Z'\ell_i\ell_i} + \sum_{S=H, \eta} a_{\ell_i}^{S\ell_i\ell_i}, \quad (58)$$

where the index  $j$  runs over the three lepton families.

## IV. NUMERICAL ANALYSIS

We now present our numerical results for the AMDM and AWMDM of the  $\tau$  lepton in the context of the SLHM. We will briefly review the existing bounds on the free parameters of the model and afterwards analyze the potential contributions to the AMDM and the AWMDM of the tau lepton for parameter values consistent with these bounds.

### A. Bounds on the parameter space of the SLHM

The SLHM parameters involved in our calculation are  $f$ ,  $t_\beta$ ,  $m_N^i$ ,  $m_\eta$ ,  $\delta_\nu$ , and the matrix elements  $V_l^{mi}$ . We will now discuss the current bounds on these parameters obtained from the study of experimental data of several observables as reported in the literature.



- As far as the symmetry breaking scale  $f$  is concerned, there are bounds arising from several observables. We list the most relevant in Table I. We can observe that the most stringent bound  $f \geq 5.6$  TeV arises from electroweak precision data (EWPD), whereas the looser bound  $f \geq 1.7$  TeV arises from parity violation in Cesium.

TABLE I: Bound on the symmetry breaking scale  $f$  of the SLHM obtained from several observables.

Observable	Lower bound on $f$ (TeV)
Parity violation in Cesium	1.7 [22]
LEP-II data	2 [22]
$Z'$ corrections to the oblique $S$ parameter	5.2 (95% C.L.) [29]
Electroweak precision data	5.6 (95% C.L.) [30]

- As for  $t_\beta$ , a fit on 21 electroweak precision observables from LEP, SLC, Tevatron, and the Higgs boson data reported by the LHC collaborations ATLAS and CMS, allowed the authors of Ref. [31] to find out the allowed region in the  $t_\beta$ - $f$  plane, which we will take into account for our numerical analysis. For the strongest bound  $f \geq 5.6$  TeV, the allowed interval of  $t_\beta$  values is 1-9. We will analyze below the dependence of the tau AMDM and AWMDM on this parameter in the allowed interval.
- In addition, the mixing angle between light and heavy neutrinos  $\delta_\nu = v/(\sqrt{2}ft_\beta)$  is experimentally constrained to be small [26], with the corresponding bound being flavor dependent:  $\delta_{\nu_e} \leq 0.03$ ,  $\delta_{\nu_\mu} \leq 0.05$ , and  $\delta_{\nu_\tau} \leq 0.09$  with 95% C.L. Since we are interested in the study of the  $\tau$  lepton, we need to make sure that we use values of  $f$  and  $t_\beta$  consistent with the bound  $\delta_\nu \leq 0.09$ , which in turn translates into the bound  $ft_\beta \gtrsim 1932$  GeV. Such a constraint is fulfilled for the values of  $f$  and  $t_\beta$  chosen in our analysis.
- For the heavy neutrino mass, we will follow the analysis of the authors of Ref. [26], in which  $m_N$  is parametrized through the ratio  $z = m_N^2/m_X^2$ . For the most stringent limit  $f = 5.6$  TeV,  $m_N \geq 0.836$  (2.644) TeV, corresponding to the value  $z = 0.1$  ( $z = 1$ ), as observed in Fig. 3. However, the tau AMDM and AWMDM contributions arising from Feynman diagrams with internal  $m_N$  have little sensitivity to a moderate change in the value of  $z$ . Therefore, we will use  $z = 1$ , namely,  $m_N = m_X$ .
- Another parameter involved in our calculation is the pseudoscalar mass  $m_\eta$ , which is basically dependent on the  $\mu$  parameter ( $m_\eta \sim \mu$ ) appearing in the scalar potential via the term  $-\mu^2(\Phi_1^\dagger \Phi_2 + H.c.)$ . In our analysis we will explore values consistent with the lower bound  $m_\eta \leq 7$  GeV, which arises from the non-observation of the  $\Upsilon \rightarrow \eta\gamma$  decay [32]. Although the dominant contribution to the AMDM can arise from a very light pseudoscalar, with mass of the order of 10 GeV, this requires relatively large values of  $t_\beta$ , which are already excluded according to the above discussion [31].
- Finally, we will assume that there is no mixing between lepton families, so we will take for simplicity  $V_\ell^{mi} = \text{diag}\{1, 1, 1\}$ .

In conclusion, we will use the set of values shown in Table II for the SLHM parameters involved in our numerical analysis. We have found that except for  $f$  and  $t_\beta$  there is little sensitivity of the AMDM and AWMDM to a mild change in the values of the remaining parameters as far as they keep between the allowed intervals. So, we will only examine the dependence of the tau AMDM and AWMDM on  $f$  and  $t_\beta$ .

TABLE II: Values used in our numerical analysis for the parameters involved in the AMDM and AWMDM of the tau lepton.

Parameter	Value
$f$	2–5 TeV
$t_\beta$	1–9
$m_N$	$\sim m_X$
$m_\eta$	20 GeV
$\delta_\nu = \frac{v}{\sqrt{2}ft_\beta}$	$\leq 0.09$
$V_\ell^{il}$	$\text{diag}\{1, 1, 1\}$

In order to estimate the tau AMDM we used the Mathematica numerical routines to evaluate the parametric integrals involved in our calculation. A cross-check was done by evaluating the results expressed in terms of Passarino-Veltman

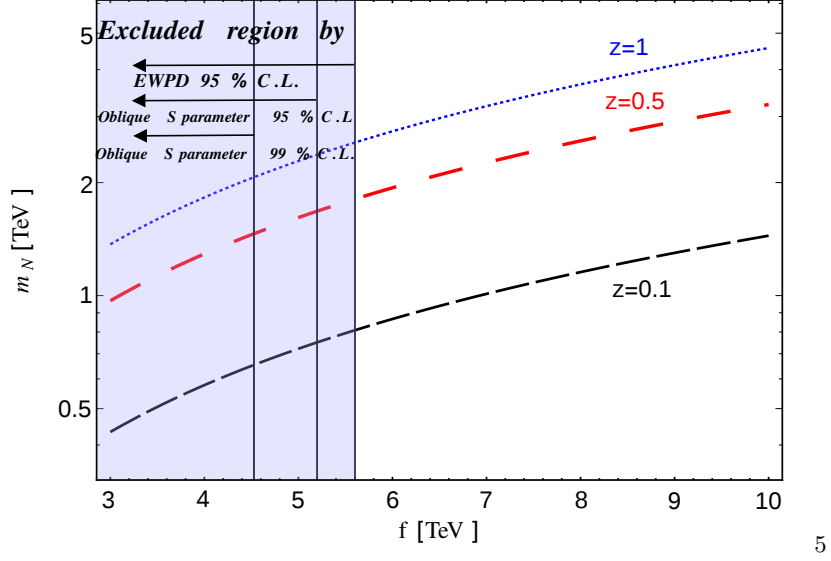


FIG. 3: Heavy neutrino mass as a function of  $f$  for  $t_\beta = 9$  and three values of  $z = m_N^2/m_X^2$ . The vertical lines represent the lower bounds on  $f$  arising from several observables.

scalar functions via the numerical FF/LoopTools routines [33, 34]. As already mentioned, it is convenient to analyze the behavior of the AMDM and AWMDM as functions of the symmetry breaking scale  $f$  since the mass of the new particles and the corrections to the SM couplings and particle masses depend on it. Also, since the mixing angle  $\delta_\nu$  depends on  $t_\beta$ , it is worth examining the dependence on this parameter in the allowed interval.

### B. Anomalous magnetic dipole moment of the $\tau$ lepton

In the left plot of Fig. 4 we show the absolute values of the main partial contributions to  $a_\tau^{NP}$  along with the total sum as a function of  $f$  for  $t_\beta = 9$ , whereas in the right plot we set  $f = 4$  TeV and show the dependence of  $a_\tau^{NP}$  on  $t_\beta$ . For the remaining parameters we use the values shown in Table II. We have refrained from showing the most suppressed contributions in these plots.

We first discuss the behavior observed in Fig. 4(a). Notice that the magnitude of each contribution depends highly on the respective  $f_\gamma^{A_1 A_2 A_3}$  coefficient and to a lower extent on the magnitude of the loop integral, which in turn dictates its behavior. Therefore, the  $\nu_\tau XX$ ,  $N_\tau WW$ , and  $\nu_\tau WW$  contributions, which are not shown in the plot, are the most suppressed ones, with values below the  $10^{-10}$  level. This stems from the fact that the  $f_\gamma^{A_1 A_2 A_3}$  coefficients associated with these contributions include two powers of the coupling constants  $g_L^{Vn\ell}$ , which are of the order of  $\delta_\nu \sim v/f$ , thereby being considerably suppressed for large  $f$ . Although the  $H\tau\tau$  and  $Z'\tau\tau$  contributions are less suppressed, they are below the  $10^{-9}$  level, whereas the  $\eta\tau\tau$  and  $N_\tau XX$  contributions are the largest ones and can reach values up to the order of  $10^{-8}$  for  $f$  around 2 TeV, which is a result of the fact that the respective  $f_\gamma^{A_1 A_2 A_3}$  coefficients have no  $(v/f)^2$  suppression factor. Another point worth to mention is that all the partial contributions are negative except for the  $H\tau\tau$  and  $N_\tau WW$  ones. Since these contributions are relatively small, they will not interfere with the dominant contributions, which will add up constructively. In conclusion both  $\eta\tau\tau$  and  $N_\tau XX$  contributions will represent the bulk of the total contribution to  $a_\tau^{NP}$ , which is of the order of  $10^{-8}$  for  $f = 2$  TeV, but has a decrease of about one order of magnitude as  $f$  increases up to 6 TeV, as observed in the plot.

We now turn to discuss the dependence of  $a_\tau^{NP}$  on the  $t_\beta$  parameter as depicted in Fig. 4(b). We observe that the  $N_\tau XX$  contribution, which does not depend on  $t_\beta$  indeed, is the dominant one, with marginal contributions arising from other diagrams. In the allowed  $t_\beta$  interval, the  $H\tau\tau$  contribution is negligible and is thus not shown in the plot. For low  $t_\beta$ , the  $\nu_\tau WW$  and  $N_\tau WW$  contributions can be as large as the  $N_\tau XX$  one, but the  $\eta\tau\tau$  contribution is the one that becomes important when  $t_\beta$  increases. Since these contributions are directly proportional to the square of the mixing parameter  $\delta_\nu = v/(\sqrt{2}t_\beta f)$ , they get suppressed by two orders of magnitude as  $t_\beta$  goes from 1 to 9. We observe that the total contribution of the SLHM to  $a_\tau^{NP}$  remains almost constant in this  $t_\beta$  interval as it is dominated by the  $N_\tau XX$  contribution.

All the above discussed properties of the SLHM contribution to  $a_\tau^{NP}$  are best illustrated in Fig. 5, where we plot the contours of  $|a_\tau^{NP}|$  in the  $f$  vs  $t_\beta$  plane for the parameter values of Table II. We observe that the SLHM contribution

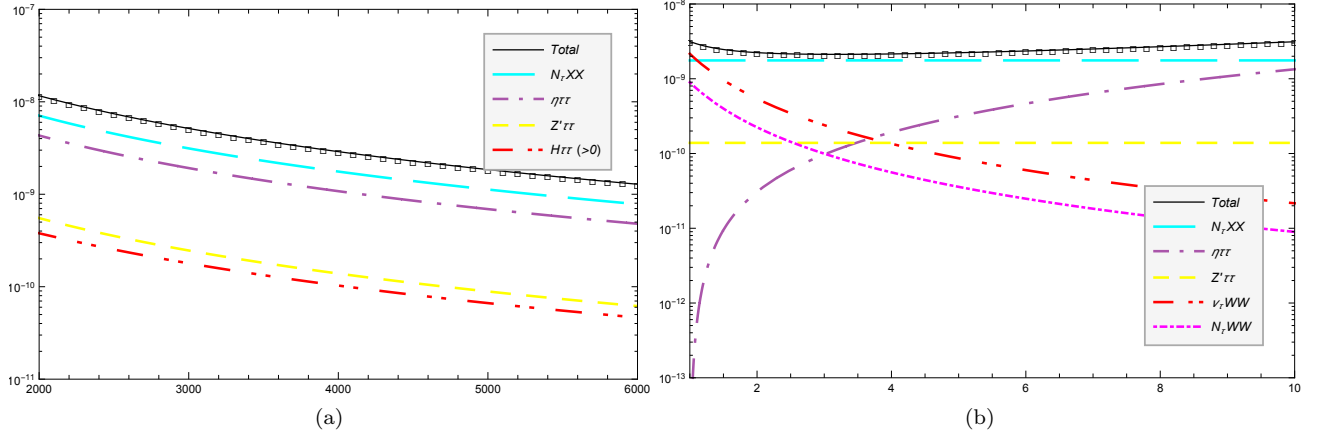


FIG. 4: Absolute values of the main partial contributions from the SLHM to  $a_\tau^{NP}$  as functions of  $f$  for  $t_\beta = 9$  (left plot) and as functions of  $t_\beta$  for  $f = 4$  TeV (right plot). For the remaining parameters of the model we use the values shown in Table II. The partial contributions below the  $10^{-10}$  level are not shown in the plots. The three-letter tags denote the virtual particles circulating in each type of Feynman diagram. All the contributions are negative except those marked by a ( $> 0$ ) label next to their corresponding tags. The absolute value of the sum all of the contributions is also shown (solid lines with squares).

to  $a_\tau^{NP}$  is of the order of  $10^{-8}$  for  $f$  between 2 TeV and 5 TeV, whereas for  $f$  above 5 TeV it is below  $10^{-9}$  and decreases rapidly as  $f$  increases. So, if we consider the most stringent constraint on  $f$ , namely 5.6 TeV, we can expect values of  $a_\tau^{NP}$  of the order of  $10^{-9}$ . We also observe that there is little dependence of  $a_\tau^{NP}$  on the value of  $t_\beta$ , but such dependence is more marked for large  $f$ . It is interesting to make a comparison with the typical predictions of some popular extension models as reported in the literature. In this respect, several extension models predict values for  $a_\tau^{NP}$  lying in the interval between  $10^{-9}$  and  $10^{-6}$  [35–38] (the theoretical prediction of the SM is of the order  $10^{-3}$ ). We note that although the SLHM contribution is of the same order than the potential contribution of leptoquark models (LQM) [35], it is disfavored with respect to the contributions of two-Higgs doublet models (THDM) [39, 40], the minimal supersymmetric standard model (MSSM) [41, 42], and unparticles (UP)[36], which can reach values as high as  $10^{-6}$ .

### C. Anomalous weak magnetic dipole moment of the $\tau$ lepton

We now present the analysis of the behavior of the NP contribution of the SLHM to the AWMDM of the tau lepton. There are some differences with respect to the AMDM: apart that the AWMDM has some additional contributions, it can now develop an imaginary part arising from those diagrams where the external  $Z$  gauge boson is attached to a pair of particles with a total mass lower than  $m_Z$ , as occurs when there are two internal SM neutrinos or tau leptons. Again, the magnitude of each contribution is highly dependent on the respective  $f_Z^{A_1 A_2 A_3}$  coefficient, whereas its behavior is dictated by that of the loop integral. We show in Fig. 6 the real part of the main partial contributions of the SLHM to  $a_\tau^{W-NP}$  and the total sum as functions of  $f$  for  $t_\beta = 9$  (left plot) and as functions of  $t_\beta$  for  $f = 4$  TeV (right plot). For the remaining parameters we use the same set of values used in our analysis of the AMDM. All the contributions not shown in the plots are negligible.

We first discuss the behavior of  $\text{Re}[a_\tau^{W-NP}]$  as a function of  $f$  as shown Fig. 6(a). Numerical evaluation shows that for  $f$  around 2 TeV the magnitude of the partial contributions ranges from  $10^{-14}$  to  $10^{-9}$ , with an additional suppression of at least one order of magnitude for  $f$  around 5 TeV. The most suppressed contributions are the  $\nu_\tau XX$ ,  $X\nu_\tau\nu_\tau$  and  $WN_\tau N_\tau$  ones, which are proportional to the  $(v/f)^2$  factor and are below the  $10^{-13}$  level. Other contributions such as  $\tau HZ'$ ,  $\nu_\tau WW$ ,  $WN_\tau\nu_\tau$ ,  $N_\tau WW$ ,  $\eta\tau\tau$ ,  $H\tau\tau$ , and  $XXN_\tau$  are less suppressed but are also below the  $10^{-10}$  level. In fact, only the contributions shown in the plot,  $\tau HZ$ ,  $N_\tau XX$ , and  $W\nu_\tau\nu_\tau$ , are relevant for the total sum. While the  $\tau HZ$  contribution is the dominant one, the  $N_\tau XX$  contribution plays a subdominant role, which again is due to the fact that the  $f_Z^{N_\tau XX}$  coefficient is not suppressed by the  $(v/f)^2$  factor. We also observe that the  $W\nu_\tau\nu_\tau$  contribution, which together with the  $\tau HZ$  contribution are absent in the AMDM, is below the  $10^{-9}$  level. Very interestingly, the  $H\tau\tau$  and  $\eta\tau\tau$  contributions, which were not very suppressed in the AMDM case, are now negligible as they are proportional to the small  $g_V^{Z\ell\ell}$  coupling. Note also that all the contributions shown in the plot are positive except for the  $\tau HZ$  one. As a result the total contribution will have an additional suppression as

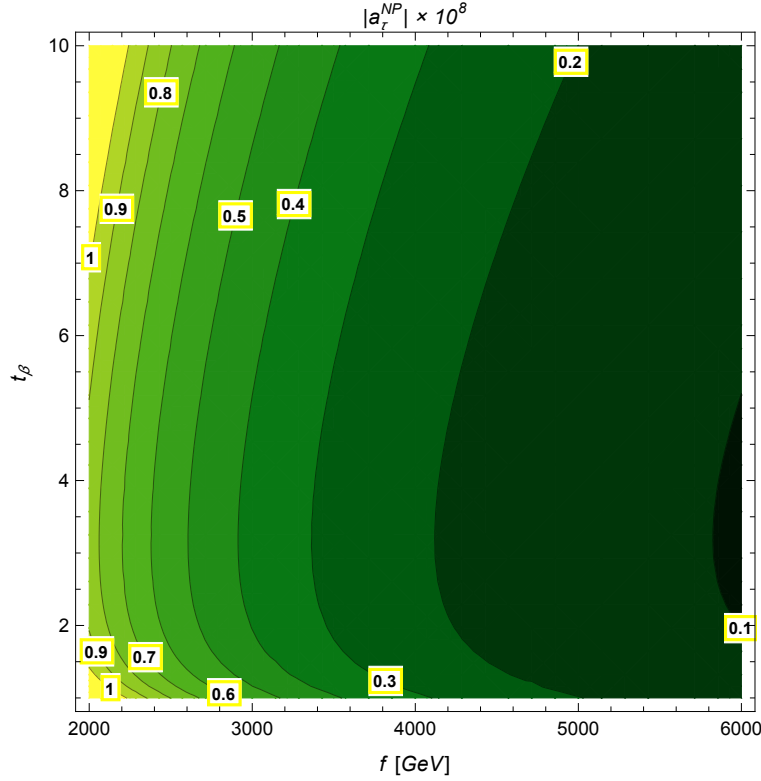


FIG. 5: Contours of the the SLHM contribution to  $|a_\tau^{NP}|$  in the  $f$  vs  $t_\beta$  plane. For the remaining parameters of the model we use the values shown in Table II.

the main contributions will have a large cancellation due to their opposite signs. This becomes evident in the curve for the total contribution, which is below that for the  $\tau HZ$  contribution.

As far as the behavior of the real part of the contributions to  $a_\tau^{W-NP}$  as a function of  $t_\beta$  is concerned, we observe in Fig. 6(b) that the  $\tau HZ$  and  $W\nu_\tau\nu_\tau$  contributions are highly dependent on  $t_\beta$ : the former increases up to one order of magnitude when  $t_\beta$  increases from 1 to 10, whereas the latter decreases one order of magnitude. On the other hand, the  $N_\tau XX$  contribution remains almost constant. Due to the opposite signs of the different contributions, there is a cancellation effect. For low  $t_\beta$ , the  $N_\tau XX$  and  $W\nu_\tau\nu_\tau$  contributions add up constructively, with the  $\tau HZ$  contribution being negligible. As  $t_\beta$  increases, the positive  $W\nu_\tau\nu_\tau$  contribution decreases while the negative  $\tau HZ$  one increases, which results in a large cancellation with the positive  $N_\tau XX$  contribution. Such a destructive interference is maximal for  $t_\beta$  around 6.8, where  $a_\tau^{W-NP}$  is negligibly small. After this point the  $\tau HZ$  contribution becomes dominant. This effect is evident in the curve for the total contribution, which exhibits a large dip due to the flip of sign:  $a_\tau^{W-NP}$  goes from positive to negative.

The behavior of the real part of  $a_\tau^{W-NP}$  as a function of  $f$  and  $t_\beta$  is best illustrated in Fig. 7, where we show the contours of the real part of the total SLHM contribution to  $a_\tau^{W-NP}$  in the  $f$  vs  $t_\beta$  plane. It can be observed that the real part of  $a_\tau^{W-NP}$  reaches its largest values, of the order of  $10^{-9}$ , for low and high  $t_\beta$ , irrespective of the value of  $f$ . There is a band centered around  $t_\beta \sim 7$  where the lowest values of real part of  $a_\tau^{W-NP}$  are reached. Such a band (darkest region) widens as  $f$  increases. We observe that for  $t_\beta$  around 10, there is a slow decrease of  $\text{Re}[a_\tau^{W-NP}]$  as  $f$  increases but in general its magnitude is of the order of  $10^{-10} - 10^{-9}$ . A comparison of the SLHM contribution with typical predictions of some SM extensions, allow us to conclude the following. We note that for  $f$  up to 4 TeV, the SLHM contribution can be above the  $10^{-9}$  level and it is thus larger than the contributions predicted by THDMs, the MSSM and UP, of the order of  $10^{-10}$ , though it is lower for  $f \gtrsim 4$  TeV.

We now turn to examine the behavior of the imaginary part of the partial contributions of the SLHM to  $a_\tau^{W-NP}$ . We follow the same approach as that used for the analysis of the real part. There are only four contributions to  $a_\tau^{W-NP}$  that can develop an imaginary part. In Fig. 8(a) we show such contributions as functions of  $f$  for  $t_\beta = 9$ . Contrary to what happens with the real part, the  $W\nu_\tau\nu_\tau$  contribution is the dominant one by far, at the level of  $10^{-10}$ , with the  $\eta\tau\tau$ ,  $H\tau\tau$ , and  $Z'\tau\tau$  contributions suppressed by more than one order of magnitude. Therefore,  $a_\tau^{W-NP}$  will be completely dominated by the  $W\nu_\tau\nu_\tau$  contribution. In fact both the curves for the  $W\nu_\tau\nu_\tau$  contribution and the total contribution overlap. In this region, the imaginary part of  $a_\tau^{W-NP}$  is positive and of the order of  $10^{-10}$ ,

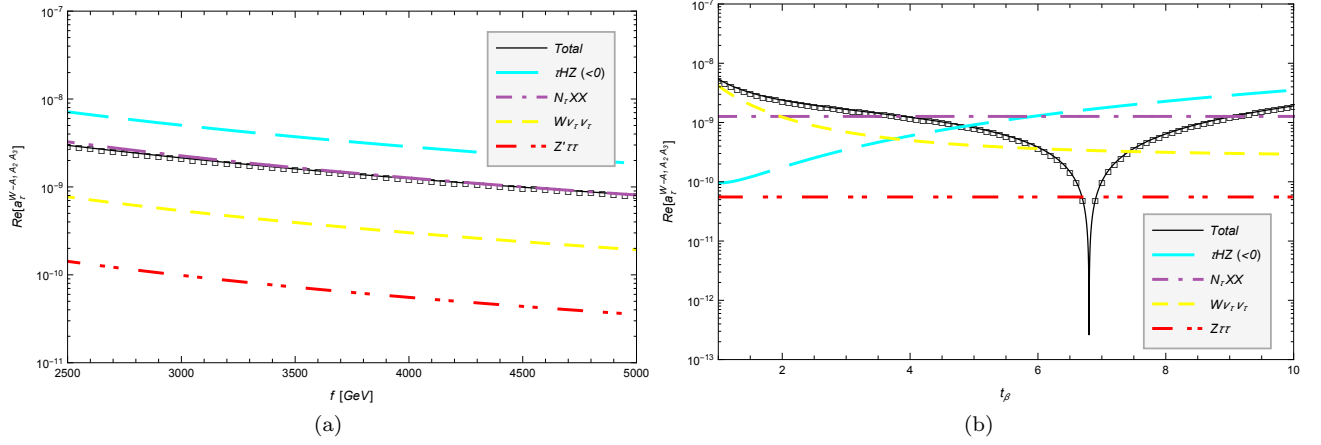


FIG. 6: Absolute value of the real part of the main partial contributions to  $a_\tau^{W-NP}$  and the total sum as a function of  $f$  for  $t_\beta = 9$  (left plot) and as a function of  $t_\beta$  for  $f = 4$  TeV. For the remaining parameters of the model we use the values of Table II. The contributions below the  $10^{-10}$  level are not shown in the plot. All the contributions are positive except those marked by a ( $< 0$ ) label next to their corresponding tags. The absolute value of the sum all of the contributions is also shown (solid lines with squares).

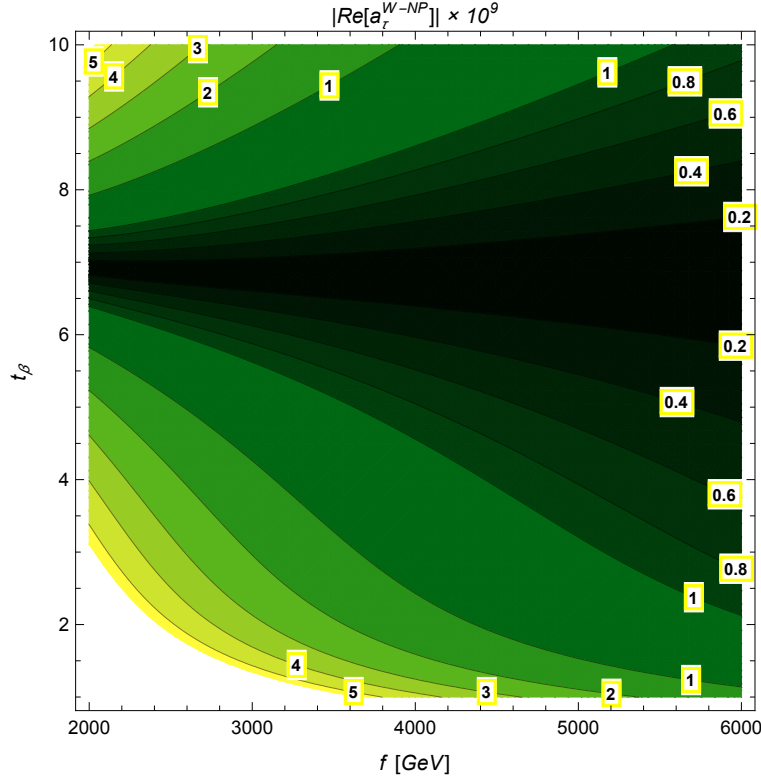


FIG. 7: Contours of the the SLHM contribution to the absolute value of the real part of  $a_\tau^{W-NP}$  in the  $f$  vs  $t_\beta$  plane. For the remaining parameters of the model we use the values shown in Table II.

with a slight decrease as  $f$  increases. As far as the behavior of the imaginary part of  $a_\tau^{W-NP}$  as a function of  $t_\beta$  [Fig. 8(b)] there is no considerable change in the analysis as in the allowed  $t_\beta$  interval the  $W\nu_\tau\nu_\tau$  contribution is dominant, whereas the remaining contributions are negligibly small. For low  $t_\beta$  the imaginary part of the total contribution to  $a_\tau^{W-NP}$  can be of the order of  $10^{-9}$ , but it goes down almost by one order of magnitude as  $t_\beta$  goes up to 10.

Finally we present the contours of the imaginary part of  $a_\tau^{W-NP}$  in the  $f$  vs  $t_\beta$  plane in Fig. 9. We observe that the imaginary part of  $a_\tau^{W-NP}$  can be of the order of  $10^{-9}$  for low values of  $t_\beta$  irrespective of the value of  $f$ , and also

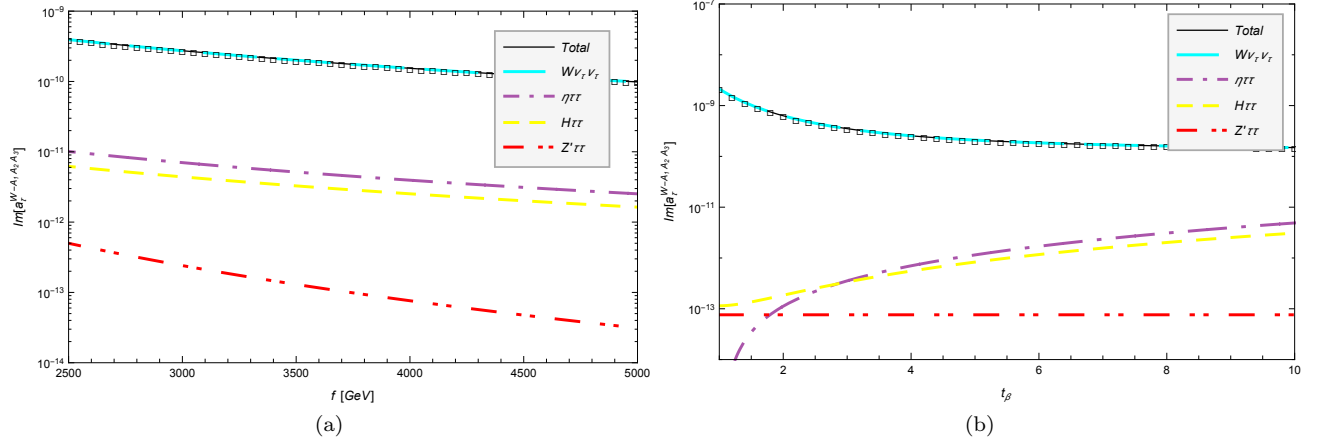


FIG. 8: The same as in Fig. 6 but for the imaginary part of  $a_\tau^{W-NP}$ .

for  $t_\beta \sim 10$  and  $f \leq 3$  TeV, but there is a marked decrease of up to one order of magnitude for larger values of  $t_\beta$  and  $f$ . We also can observe that  $\text{Im}[a_\tau^{W-NP}]$  decreases mildly as  $f$  increases. As far as the values predicted by other extension models, although the imaginary part of the total contribution of the SLHM is larger than that of LQM of type I and II, of the order of  $10^{-10}$ , it is well below the contributions predicted by THDMs and the MSSM, of the order of  $10^{-7}$ .

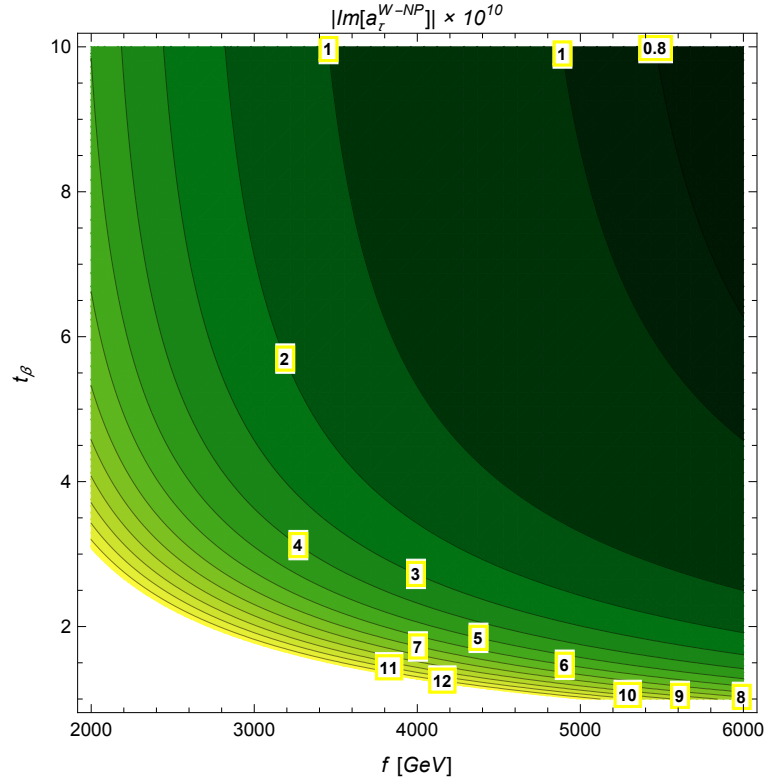


FIG. 9: The same as in Fig. 7 but for the imaginary part of  $a_\tau^{W-NP}$ .

## V. CONCLUSIONS

In this work we have calculated analytical expressions, both in terms of parametric integrals and Passarino-Veltman scalar functions, for the one-loop contributions to the static anomalous magnetic and weak magnetic dipole moments of a charged lepton in the context of the SLHM, which is a  $CP$ -conserving theory and so predicts vanishing electric and weak electric dipole moments. The expressions for the weak properties are very general and can be useful to compute the weak properties of a charged lepton in other extension models. For the numerical analysis we have focused on the case of the tau lepton since their electromagnetic and weak properties are the least studied in the literature and also because they have great potential to be experimentally tested in the future. For values of the parameters of the model allowed by current experimental data we find that the respective contribution to the tau AMDM is of the order of  $10^{-9}$ , whereas the real (imaginary) part of the tau AWMDM is of the order of  $10^{-9}$  ( $10^{-10}$ ). The SLHM contribution to the tau AMDM could have some enhancement in the scenario in which there is a very light pseudoscalar boson  $\eta$ , with a mass of the order of about 10 GeV, and  $t_\beta$  is of the order of 20. However such a value of  $t_\beta$  are already excluded according to the bounds obtained from experimental data. While the values predicted for the tau AMDM are smaller than those predicted by other extension models, the real part of the tau AWMDM can be of similar size as the predictions of THDMs and the MSSM.

## Acknowledgments

We acknowledge financial support from Sistema Nacional de Investigadores (Mexico), Consejo Nacional de Ciencia y Tecnología (Mexico) and Vicerrectoría de Investigación y Estudios de Posgrado (BUAP).

## Appendix A: Feynman Rules in the SLHM

We now present the Feynman rules necessary for our calculation (see [26] for a complete set of SLHM Feynman rules). We note that the coupling constant associated with the  $A_1 A_2 A_3$  vertex will be written as  $ieg^{A_1 A_2 A_3}$ , so the  $f_V^{A_1 A_2 A_3}$  ( $V = Z, \gamma$ ) coefficients of Eqs. (54) and (57) will be given in terms of the  $g^{A_1 A_2 A_3}$  constants. In Table III we show the Feynman rules for the trilinear gauge boson couplings  $V_i V_j^+ V_j^-$ , whereas in Table IV we show the ones for the vertices of a gauge boson to a fermion pair  $V \bar{f}_i f_j$ . Finally, Table V gathers all the Feynman rules for the scalar interactions.

TABLE III: Feynman rules for the trilinear gauge boson couplings  $V_\mu(p_1)V_\nu^+(p_2)V_\rho^-(p_3)$ . The Feynman rule for all these couplings have the generic form  $ieg^{V_i V_j V_j}(g_{\mu\nu}(p_2 - p_1)_\rho + g_{\nu\rho}(p_3 - p_2)_\mu + g_{\mu\rho}(p_1 - p_3)_\nu)$ , where the  $g^{V_i V_j V_j}$  constants are shown in the right column. All the four-momenta are taken incoming.

Vertex	$g^{V_i V_j V_j}$
$AX^+X^-$	-1
$AW^+W^-$	-1
$ZX^+X^-$	$\frac{c_W^2 - s_W^2}{2s_W c_W} - \frac{\delta_Z}{2} \frac{\sqrt{3-t_W^2}}{s_W}$
$ZW^+W^-$	$\frac{c_W}{s_W}$

## Appendix B: Loop integrals

The AWMDM and AWMDM of a lepton are given by Eqs. (54) and (57). The  $f_V^{A_1 A_2 A_3}$  coefficients are shown in Table VI and the loop functions  $I_V^{A_1 A_2 A_3 - 3}$  ( $V = Z, \gamma$ ) will be presented below. The loop integration was performed via both Feynman parametrization and the Passarino-Veltman method [43]. For the Dirac algebra and the Passarino-Veltman reduction we used the Feyncalc routines [44], and a further simplification was done with the help of the Mathematica symbolic algebra routines. We will first present the results in terms of parametric integrals.

TABLE IV: Feynman rules for the vertices of a gauge boson to a lepton pair  $V_\mu \bar{f}_i f_j$ . The Feynman rule for this class of vertices has the generic form  $ie(g_L^{V\bar{f}_i f_j} P_L + g_R^{V\bar{f}_i f_j} P_R)\gamma_\mu$ , with  $P_L$  and  $P_R$  the left- and right-chirality projectors, where the  $g_L^{V\bar{f}_i f_j}$  and  $g_R^{V\bar{f}_i f_j}$  constants are shown in the second and third columns. The vector and axial couplings are  $2g_V^{V\bar{f}_i f_j} = g_L^{V\bar{f}_i f_j} + g_R^{V\bar{f}_i f_j}$  and  $2g_A^{V\bar{f}_i f_j} = g_L^{V\bar{f}_i f_j} - g_R^{V\bar{f}_i f_j}$ .

Vertex	$g_L^{V\bar{f}_i f_j}$	$g_R^{V\bar{f}_i f_j}$
$Z\bar{\ell}\ell$	$\frac{-1+2s_W^2}{2s_W c_W} + \frac{1-2s_W^2}{2s_W c_W^2 \sqrt{3-t_W^2}} \delta_Z$	$\frac{s_W}{c_W} - \frac{s_W}{c_W^2 \sqrt{3-t_W^2}} \delta_Z$
$Z\bar{\nu}\nu$	$\frac{1}{2s_W c_W} (1 - \delta_\nu^2) + \frac{1-2s_W^2}{2s_W c_W^2 \sqrt{3-t_W^2}} \delta_Z$	0
$Z\bar{N}N$	$\frac{1}{2s_W c_W} \delta_\nu^2 - \frac{1}{s_W \sqrt{3-t_W^2}} \delta_Z$	0
$Z\bar{N}_m\nu$	$-\frac{1}{2s_W c_W} \delta_\nu V_l^{mi}$	0
$W^+\bar{\nu}\ell$	$\frac{1}{\sqrt{2}s_W} \left(1 - \frac{\delta_\nu^2}{2}\right)$	0
$W^+\bar{N}_m\ell$	$-\frac{1}{\sqrt{2}s_W} \delta_\nu V_l^{mi}$	0
$X^+\bar{\nu}\ell$	$-\frac{i}{\sqrt{2}s_W} \delta_\nu$	0
$X^+\bar{N}_m\ell$	$-\frac{i}{\sqrt{2}s_W} \left(1 - \frac{\delta_\nu^2}{2}\right) V_l^{mi}$	0
$Z'\bar{\ell}\ell$	$\frac{1-2s_W^2}{2s_W c_W^2 \sqrt{3-t_W^2}} + \frac{1-2s_W^2}{2s_W c_W} \delta_Z$	$-\frac{s_W}{c_W^2 \sqrt{3-t_W^2}} - \frac{s_W}{c_W} \delta_Z$

TABLE V: Feynman rules for the vertices involving the scalar bosons  $H$  and  $\eta$  at the leading order in  $v/f$  in the SLHM.

Vertex	Feynman rule	$g^{A_1 A_2 A_3}$
$H\bar{\ell}\ell$	$ieg^{H\bar{\ell}\ell}$	$-\frac{m_\ell}{2s_W m_W} \left(1 - \frac{v^2}{6f^2} \left(\frac{1}{t_\beta} + t_\beta\right)^2\right)$
$HZ_\alpha Z_\beta$	$ieg^{ZZH} g_{\alpha\beta}$	$\frac{gv}{2c_W s_W} \left(1 - \frac{v^2}{4f^2} \left(\frac{1}{3} \left(\frac{s_\beta^4}{c_\beta^2} + \frac{c_\beta^4}{s_\beta^2}\right) + \frac{1}{4} (1 - t_W^2)^2\right)\right)$
$\eta\bar{\ell}\ell$	$ieg^{\eta\bar{\ell}\ell} \gamma^5$	$\frac{im_\ell}{\sqrt{2}s_W f} \left(\frac{1}{t_\beta} - t_\beta\right)$
$HZ_\alpha Z'_\beta$	$ieg^{HZZ'} g_{\alpha\beta}$	$\frac{gv(1-t_W^2)}{2s_W c_W \sqrt{3-t_W^2}}$

TABLE VI: Coefficients  $f_Z^{A_1 A_2 A_3}$  and  $f_\gamma^{A_1 A_2 A_3}$  required in Eqs. (54) and (57), respectively, to compute the AWMDM and AMDM of a charged lepton arising from loops carrying the  $A_1 A_2 A_3$  particles. Here  $n$  is the SM neutrino  $\nu$  or a heavy one  $N$ . The coupling constants  $g^{A_1 A_2 A_3}$  are shown in appendix A.

$A_1 A_2 A_3$	$f_Z^{A_1 A_2 A_3}$	$f_\gamma^{A_1 A_2 A_3}$
$nVV$ ( $V = W, X$ )	$g^{ZVV} (g_L^{Vn\ell})^2$	$g^{AVV} (g_L^{V\ell n})^2$
$Z'\ell\ell$	1	1
$Vnn$ ( $V = W, X$ )	$g_L^{Znn} (g_L^{Vn\ell})^2$	—
$V\nu N$ ( $V = W, X$ )	$g_L^{ZN\nu} g_L^{V\nu\ell} g_L^{VN\ell}$	—
$S\ell\ell$ ( $S = H, \eta$ )	$g_V^{Z\ell\ell} (g^{S\ell\ell})^2$	$(g^{S\ell\ell})^2$
$\ell HV$ ( $V = Z, Z'$ )	$\frac{1}{m_Z} g^{HZV} g^{H\ell\ell} g_V^{V\ell\ell}$	—

### 1. Parametric integrals

Once Feynman parametrization is applied, the  $I_V^{A_1 A_2 A_3}$  loop integrals can be cast in the following form after one parameter is integrated out:



$$I_V^{A_1 A_2 A_3} = \int_0^1 F_V^{A_1 A_2 A_3}(x) dx. \quad (B1)$$

We will first present the  $F_Z^{A_1 A_2 A_3}(x)$  functions necessary to calculate the AWMDM of a lepton.

*a. Anomalous weak magnetic dipole moment*

We start by introducing the functions

$$f_1^{A_1 A_2 A_3}(x) = \frac{1}{\sqrt{Z^{A_1 A_2 A_3}(x)}} \arctan \left[ \frac{X^{A_1 A_2 A_3}(x)}{\sqrt{Z^{A_1 A_2 A_3}(x)}} \right], \quad (B2)$$

and

$$f_2^{A_1 A_2 A_3}(x) = \log [Y^{A_1 A_2 A_3}(x)]. \quad (B3)$$

For diagram (1) we obtain

$$\begin{aligned} F_Z^{nVV}(x) = & x_\ell \left[ x \left( (3x(2-x) - 2)x_Z + 6x^2 - 8x + 2 \right) + \frac{1}{2}x \left( (4x^2 - 9x + 4)x_Z - 8x^2 + 12x - 4 \right) f_2^{nVV}(x) \right. \\ & + \left( 2 \left( x^3(x_Z - 2)(x_n + x_\ell - 1) + x^2(2x_n(3 - 2x_Z) - 2(x_Z - 1)x_\ell + 3x_Z - 8) \right. \right. \\ & + \left. \left. x(x_n(5x_Z - 4) + x_Z x_\ell - 2) - 2x_n x_Z \right) + Z^{nVV}(x) \left( 4x^2(x_Z - 2) + x(12 - 9x_Z) + 4(x_Z - 1) \right) \right) \\ & \left. \times f_1^{nVV}(x) \right], \end{aligned} \quad (B4)$$

with

$$X^{nVV}(x) = xx_Z, \quad (B5)$$

$$Y^{nVV}(x) = (1-x)(x_n - xx_\ell) + x, \quad (B6)$$

$$Z^{nVV}(x) = x_Z(4Y^{nVV}(x) - x^2 x_Z), \quad (B7)$$

where we have introduced the dimensionless variable  $x_a = (m_a/m_V)^2$ .

As for the contribution of diagram (2), the  $F_Z^{Z'\ell\ell}$  function can be written as

$$F_Z^{Z'\ell\ell} = \left(g_L^{Z'\ell\ell}\right)^2 F_{Z-L}^{Z'\ell\ell} + \left(g_R^{Z'\ell\ell}\right)^2 F_{Z-R}^{Z'\ell\ell} + g_L^{Z'\ell\ell} g_R^{Z'\ell\ell} F_{Z-LR}^{Z'\ell\ell}, \quad (B8)$$

with

$$\begin{aligned} F_{Z-L}^{Z'\ell\ell}(x) = & y_\ell \left[ 2x(2x-1)g_L^{Z\ell\ell} - x(3x-2)g_L^{Z\ell\ell} f_2^{Z'\ell\ell}(x) \right. \\ & \left. - 2 \left( \left( 2x^2 y_\ell + 6x^2 + 6(2-3x) + Z^{Z'\ell\ell}(x)(3x-2) \right) g_L^{Z\ell\ell} + 2x^2 y_\ell g_R^{Z\ell\ell} \right) f_1^{Z'\ell\ell}(x) \right] \end{aligned} \quad (B9)$$

$$F_{Z-R}^{Z'\ell\ell}(x) = F_{Z-L}^{Z'\ell\ell}(x) (g_L^{Z\ell\ell} \leftrightarrow g_R^{Z\ell\ell}), \quad (B10)$$

and

$$\begin{aligned} F_{Z-LR}^{Z'\ell\ell}(x) = & y_\ell (g_L^{Z\ell\ell} + g_R^{Z\ell\ell}) \left[ 2(1-2x)x + x(3x-2)f_2^{Z'\ell\ell}(x) \right. \\ & \left. + 2 \left( 2x^2(2y_\ell + 1) - 14x + Z^{Z'\ell\ell}(x)(3x-2) + 12 \right) f_1^{Z'\ell\ell}(x) \right], \end{aligned} \quad (B11)$$

with  $y_a = (m_a/m_{Z'})^2$  and

$$X^{Z'\ell\ell}(x) = xy_Z, \quad (\text{B12})$$

$$Y^{Z'\ell\ell}(x) = x^2y_\ell - x + 1, \quad (\text{B13})$$

$$Z^{Z'\ell\ell}(x) = y_Z \left( 4Y^{Z'\ell\ell}(x) - x^2y_Z \right). \quad (\text{B14})$$

We now present the contribution of diagram (3):

$$\begin{aligned} F_Z^{Vnn}(x) = & x_\ell \left[ 2x(2x-1) + (2-3x)x f_2^{Vnn}(x) \right. \\ & \left. + \left( 4x^2(x_n - 2x_\ell - 3) + 4x(2(x_\ell - x_n) + 9) + 2Z^{Vnn}(x)(2-3x) - 24 \right) f_1^{Vnn}(x) \right], \end{aligned} \quad (\text{B15})$$

with

$$X^{Vnn}(x) = xx_Z, \quad (\text{B16})$$

$$Y^{Vnn}(x) = x(x_n - x_\ell - 1) + x^2x_\ell + 1, \quad (\text{B17})$$

$$Z^{Vnn}(x) = x_Z (Y^{Vnn}(x) - x^2x_Z). \quad (\text{B18})$$

Finally, the loop function arising from diagram (4) is given by

$$\begin{aligned} F_Z^{V\nu N}(x) = & \frac{x_\ell}{x_Z} \left[ 4x(2x-1)x_Z + 2xx_N (f_{21}^{V\nu N}(x) - f_{22}^{V\nu N}(x)) + x(2-3x)x_Z (f_{21}^{V\nu N}(x) + f_{22}^{V\nu N}(x)) \right. \\ & + 2\sqrt{x_Z} \left( (x-2)xx_Nx_Z - (x-2)x_N^2 - (3x-2)Z^{Vnn}(x) - 2(x-1)x_Z(2xx_\ell + 3x-6) \right) \\ & \left. \times (f_{11}^{V\nu N}(x) + f_{12}^{V\nu N}(x)) \right], \end{aligned} \quad (\text{B19})$$

where the functions  $f_{1a}^{A_1A_2A_3}(x)$  and  $f_{2a}^{A_1A_2A_3}(x)$  are obtained from  $f_1^{A_1A_2A_3}(x)$  and  $f_2^{A_1A_2A_3}(x)$  after the replacement  $X^{A_1A_2A_3}(x) \rightarrow X_a^{A_1A_2A_3}(x)$  and  $Y^{A_1A_2A_3}(x) \rightarrow Y_a^{A_1A_2A_3}(x)$ , respectively. In addition

$$X_1^{V\nu N}(x) = xx_Z - x_n, \quad (\text{B20})$$

$$X_2^{V\nu N}(x) = xx_Z + x_n, \quad (\text{B21})$$

$$Y_1^{V\nu N}(x) = (x-1)(xx_\ell - 1), \quad (\text{B22})$$

$$Y_2^{V\nu N}(x) = x(x_n - x_\ell - 1) + x^2x_\ell + 1, \quad (\text{B23})$$

$$Z^{V\nu N}(x) = 4Y_2^{V\nu N}(x) - x^2x_Z. \quad (\text{B24})$$

We now turn to the parametric integrals for the diagrams of Fig. 2. For diagram (1) we obtain

$$F_Z^{H\ell\ell}(x) = -8x(2-x)w_\ell f_1^{H\ell\ell}(x), \quad (\text{B25})$$

with  $w_a = (m_a/m_H)^2$  and

$$X^{H\ell\ell}(x) = xw_Z, \quad (\text{B26})$$

$$Z^{H\ell\ell}(x) = w_Z \left( (4(1-x(1-xw_\ell^2)) - w_Zx^2) \right). \quad (\text{B27})$$

Also, for the contribution of the pseudoscalar  $\eta$  we obtain

$$F_Z^{\eta\ell\ell}(x) = 8x^2z_\ell f_1^{\eta\ell\ell}(x), \quad (\text{B28})$$

with  $z_a = (m_a/m_\eta)^2$ ,  $X^{\eta\ell\ell}(x) = X^{H\ell\ell}(x)[w_a \rightarrow z_a]$ , and  $Z^{\eta\ell\ell}(x) = Z^{H\ell\ell}(x)[w_a \rightarrow z_a]$ .

As for the contribution of diagram (2) and the one obtained by exchanging the internal gauge boson with the scalar boson, it is as follows

$$\begin{aligned}
F_Z^{\ell HV}(x) = & \frac{\sqrt{x_\ell}}{\sqrt{x_Z}} \left[ 4x(1-2x)x_Z + ((1-2x)x_H + 2x-3) (f_{21}^{\ell HV}(x) - f_{22}^{\ell HV}(x)) \right. \\
& + (3x-2)xx_Z (f_{21}^{\ell HV}(x) + f_{22}^{\ell HV}(x)) - 2\sqrt{x_Z} (x^2x_Z(5x_H + 2x_Z - 28x_\ell + 5) \\
& - x(x_H(3x_Z - 4) + 2x_H^2 - 20x_Zx_\ell + 5x_Z + 2) + x_H(x_H - 4) + 3x^3x_Z(4x_\ell - x_Z) - 4x_Zx_\ell + 3) \\
& \left. \times (f_{11}^{\ell HV}(x) - f_{12}^{\ell HV}(x)) \right], \tag{B29}
\end{aligned}$$

where

$$X_1^{\ell HV}(x) = x_H - xx_Z - 1, \tag{B30}$$

$$X_2^{\ell HV}(x) = x_H + xx_Z - 1, \tag{B31}$$

$$Y_1^{\ell HV}(x) = x^2x_\ell - 2xx_\ell + x_\ell + x, \tag{B32}$$

$$Y_2^{\ell HV}(x) = x^2x_\ell - 2xx_\ell + x_\ell + xx_H, \tag{B33}$$

$$Z^{\ell HV}(x) = 2x_H(xx_Z + 1) - x_H^2 + x^2x_Z(4x_\ell - x_Z) + xx_Z(2 - 8x_\ell) + 4x_Zx_\ell - 1. \tag{B34}$$

### b. Anomalous magnetic dipole moment

For completeness we present the contributions to the AMDM, which can be obtained from those to the AWMDM expressions after taking the limit  $m_Z \rightarrow 0$  and substituting the  $Z$  coupling constants by the photon ones. The  $f_{\gamma}^{A_1 A_2 A_3}$  coefficients of Eq. (57) are presented in Table VI, whereas the respective loop integrals are of the form of (B1).

As far as Fig. 1 is concerned, there are only contributions from diagrams (1) and (2), but with the external  $Z$  gauge boson replaced by the photon. The contribution of diagram (1) can be written as

$$F_{\gamma}^{nVV}(x) = -\frac{xx_\ell}{Y^{nV}(x)} (x^2(x_n + x_\ell + 2) - x(3x_n + x_\ell - 2) + 2x_n). \tag{B35}$$

As for the contribution of diagram (2), the  $F_{\gamma}^{Z'\ell\ell}$  function is given by an analogous expression to Eq. (B8) but now  $F_{\gamma-R}^{Z'\ell\ell}(x) = F_{\gamma-L}^{Z'\ell\ell}(x)$ , with

$$F_{\gamma-L}^{Z'\ell\ell}(x) = -\frac{2xy_\ell}{Y^{Z'\ell\ell}(x)} (x^2(y_\ell + 1) - 3x + 2), \tag{B36}$$

and

$$F_{\gamma-LR}^{Z'\ell\ell}(x) = \frac{4xy_\ell}{Y^{Z'\ell\ell}(x)} (x^2y_\ell - 2(x-1)). \tag{B37}$$

In the limit of small  $x_\ell$  the integration of the above functions is straightforward and one obtains

$$I_{\gamma}^{nVV} = -\frac{x_\ell}{6(1-x_n)^4} ((1-x_n)(10-x_n(33+x_n(4x_n-45))) + 18x_n^3 \log(x_n)), \tag{B38}$$

$$I_{\gamma-LR}^{Z'\ell\ell} = -3I_{\gamma-L}^{Z'\ell\ell} = 4y_\ell. \tag{B39}$$

Finally, there are also contribution of the scalar bosons  $H$  and  $\eta$  arising from the diagram (1) of Fig. 2, with the  $Z$  gauge boson replaced by the photon. The respective  $F_{\gamma}^{A_1 A_2 A_3}(x)$  functions can be written as

$$F_{\gamma}^{H\ell\ell}(x) = \frac{2x^2(2-x)w_\ell}{w_\ell x^2 + 1 - x}, \tag{B40}$$

and

$$F_{\gamma}^{\eta\ell\ell}(x) = \frac{2x^3z_\ell}{z_\ell x^2 + 1 - x}. \tag{B41}$$

All of the above results agree with previous calculations of the AMDM of a lepton (see for instance [7, 45]).

## 2. Passarino-Veltman scalar functions

We now present the results for the AWMDM and AMDM of a lepton in terms of Passarino-Veltman scalar functions.

### a. Anomalous weak magnetic dipole moment

We first introduce the following ultraviolet finite functions given in terms of two-point Passarino-Veltman scalar integrals:

$$\Delta_1 = B_0(0, m_N^2, m_V^2) - B_0(m_\ell^2, m_N^2, m_V^2), \quad (\text{B42})$$

$$\Delta_2 = B_0(m_Z^2, m_V^2, m_V^2) - B_0(m_\ell^2, m_N^2, m_V^2), \quad (\text{B43})$$

$$\Delta_3 = B_0(0, m_\ell^2, m_{Z'}^2) - B_0(m_\ell^2, m_\ell^2, m_{Z'}^2), \quad (\text{B44})$$

$$\Delta_4 = B_0(m_Z^2, m_\ell^2, m_\ell^2) - B_0(m_\ell^2, m_\ell^2, m_{Z'}^2), \quad (\text{B45})$$

$$\Delta_5 = B_0(m_Z^2, m_N^2, m_N^2) - B_0(m_\ell^2, m_N^2, m_V^2), \quad (\text{B46})$$

$$\Delta_7 = B_0(m_\ell^2, 0, m_V^2) - B_0(m_Z^2, 0, m_N^2), \quad (\text{B47})$$

$$\Delta_8 = B_0(m_Z^2, 0, m_N^2) - B_0(0, 0, m_V^2), \quad (\text{B48})$$

and use a shorthand notation for the following three-point scalar functions

$$C_1 = m_V^2 C_0(m_\ell^2, m_\ell^2, m_Z^2, m_V^2, m_N^2, m_V^2), \quad (\text{B49})$$

$$C_2 = m_{Z'}^2 C_0(m_\ell^2, m_\ell^2, m_Z^2, m_\ell^2, m_{Z'}^2, m_\ell^2), \quad (\text{B50})$$

$$C_3 = m_V^2 C_0(m_\ell^2, m_\ell^2, m_Z^2, m_N^2, m_V^2, m_N^2), \quad (\text{B51})$$

$$C_4 = m_V^2 C_0(m_\ell^2, m_\ell^2, m_Z^2, m_N^2, m_V^2, 0). \quad (\text{B52})$$

The  $I_Z^{A_1 A_2 A_3}$  loop functions arising from the diagrams of Fig. 1 are given as follows. For diagram (1) we obtain

$$\begin{aligned} I_Z^{nVV} = & \frac{x_\ell}{2(x_Z - 4x_\ell)^2} \left[ (4x_\ell - x_Z) ((x_n + x_\ell)(x_Z - 2) - 4) \right. \\ & - \frac{1}{x_\ell} (x_n - 1) (4x_\ell - x_Z) ((x_n + x_\ell)(x_Z - 2) - 4) \Delta_1 \\ & - \left( x_\ell (x_Z (x_Z + 8) - 60) + 2(x_n (3x_n - 4x_\ell) + x_\ell^2) (x_Z - 2) \right. \\ & + \left. x_n (x_Z (5x_Z - 16) - 12) - 4(x_Z (x_Z - 3) - 6) \right) \Delta_2 \\ & + 2 \left( x_\ell^2 (24 - 5x_n (x_Z - 2) - x_Z (x_Z + 4)) \right. \\ & + x_\ell (7x_n^2 (x_Z - 2) + x_n (3x_Z^2 - 14x_Z + 24) + 3x_Z^2 - x_Z - 34) \\ & - 3x_n^3 (x_Z - 2) + 2x_n^2 (7 - 2x_Z) x_Z - x_n (x_Z^3 - 7x_Z^2 + 9x_Z + 18) \\ & \left. \left. + x_\ell^3 (x_Z - 2) - 2x_Z^2 + 4x_Z + 12 \right) C_1 \right], \end{aligned} \quad (\text{B53})$$

whereas the loop function arising from diagram (2) is given by a similar expression to Eq. (B8):

$$I_Z^{Z'\ell\ell} = \left( g_L^{Z'\ell\ell} \right)^2 I_{Z-L}^{Z'\ell\ell} + \left( g_R^{Z'\ell\ell} \right)^2 I_{Z-R}^{Z'\ell\ell} + g_L^{Z'\ell\ell} g_R^{Z'\ell\ell} I_{Z-LR}^{Z'\ell\ell}, \quad (\text{B54})$$

where

$$\begin{aligned}
I_{Z-L}^{Z'\ell\ell} = & -\frac{2y_\ell}{(y_Z - 4y_\ell)^2} \left[ (4y_\ell - y_Z) (g_L^{Z\ell\ell} (y_\ell + 2) + g_R^{Z\ell\ell} y_\ell) \right. \\
& + \frac{1}{y_\ell} (y_\ell - 1) (4y_\ell - y_Z) (g_L^{Z\ell\ell} (y_\ell + 2) + g_R^{Z\ell\ell} y_\ell) \Delta_3 \\
& - (g_L^{Z\ell\ell} (y_\ell (4y_\ell - (y_Z + 34)) + 2(5y_Z + 6)) + g_R^{Z\ell\ell} y_\ell (4y_\ell - y_Z + 6)) \Delta_4 \\
& \left. + 2(4y_\ell - y_Z - 3) (g_L^{Z\ell\ell} (2 - 7y_\ell + 2y_Z) + g_R^{Z\ell\ell} y_\ell) C_2 \right], \tag{B55}
\end{aligned}$$

$$I_{Z-R}^{Z'\ell\ell} = I_{Z-L}^{Z'\ell\ell} (g_L^{Z\ell\ell} \leftrightarrow g_R^{Z\ell\ell}), \tag{B56}$$

and

$$\begin{aligned}
I_{Z-LR}^{Z'\ell\ell} = & \frac{2y_\ell (g_L^{Z\ell\ell} + g_R^{Z\ell\ell})}{(y_Z - 4y_\ell)^2} \left[ y_\ell (4y_\ell - y_Z) + (y_\ell - 1) (4y_\ell - y_Z) \Delta_3 \right. \\
& - (y_\ell (4y_\ell - (y_Z + 10)) + 4y_Z) \Delta_4 \\
& \left. - 2(y_\ell (12y_\ell - (7y_Z + 5)) + y_Z (y_Z + 2)) C_2 \right]. \tag{B57}
\end{aligned}$$

As for diagram (3), the respective loop integral is

$$\begin{aligned}
I_Z^{Vnn} = & \frac{x_\ell}{(x_Z - 4x_\ell)^2} \left[ (x_\ell + 2) (x_Z - 4x_\ell) + \frac{1}{x_\ell} (x_n - 1) (x_\ell + 2) (x_Z - 4x_\ell) \Delta_1 \right. \\
& + (x_\ell (2x_n + x_Z - 22) - 2(x_n (x_Z + 6) - 5x_Z - 6) + 2x_\ell^2) \Delta_5 \\
& + 2(x_\ell^2 (2x_n + x_Z + 12) - x_\ell (2x_n (x_Z - 5) + x_n^2 + 8x_Z + 17) \\
& \left. + x_n^2 (x_Z + 6) - x_n (7x_Z + 12) - x_\ell^3 + 2(x_Z^2 + 4x_Z + 3)) C_3 \right]. \tag{B58}
\end{aligned}$$

Finally, the loop function arising from diagram (4) obeys

$$\begin{aligned}
I_Z^{V\nu n} = & \frac{1}{(x_Z - 4x_\ell)^2 x_Z} \left[ 2x_\ell x_Z (x_\ell + 2) (x_Z - 4x_\ell) + x_Z (x_n - 1) (x_\ell + 2) (x_Z - 4x_\ell) \Delta_1 \right. \\
& - (2x_\ell^3 (6x_n + x_Z) + x_\ell^2 ((x_Z - 18) x_Z - 2x_n (3x_Z + 4)) + x_\ell x_Z (20 - 4x_n + 9x_Z) - 2x_Z^2) \Delta_6 \\
& + (2x_\ell^3 (x_Z - 6x_n) + x_\ell^2 (8x_n (x_Z + 1) + (x_Z - 26) x_Z) + x_Z x_\ell (4 - 2x_n (x_Z + 4) + 11x_Z) + 2x_Z^2) \Delta_7 \\
& - x_\ell (2x_\ell^2 (x_Z - 6x_n) + x_\ell (8x_n (x_Z + 1) + (x_Z - 22) x_Z) - 2x_Z (x_n (x_Z + 4) - 5x_Z - 6)) \Delta_8 \\
& + 2x_\ell (x_\ell^2 (2x_n (x_Z - 3x_n) + 2x_Z (x_Z + 12)) + x_\ell (x_n^2 (3x_Z + 4) - 2x_Z (x_n (x_Z - 5) + (8x_Z + 17))) \\
& \left. - x_Z (x_n (7x_Z + 12) - 2x_n^2 - 4(x_Z^2 + 4x_Z + 3)) - 2x_\ell^3 x_Z) C_4 \right]. \tag{B59}
\end{aligned}$$

We now present the loop functions for the diagrams of Fig. 2. We will use the following additional Passarino-Veltman scalar functions

$$\Delta_9 = B_0(0, m_H^2, m_\ell^2) - B_0(m_Z^2, m_\ell^2, m_\ell^2), \tag{B60}$$

$$\Delta_{10} = B_0(m_\ell^2, m_H^2, m_\ell^2) - B_0(m_Z^2, m_\ell^2, m_\ell^2), \tag{B61}$$

$$C_5 = m_H^2 C_0(m_\ell^2, m_\ell^2, m_Z^2, m_\ell^2, m_H^2, m_\ell^2). \tag{B62}$$

For diagram (1) we obtain for the contribution of the SM Higgs boson  $H$

$$I_Z^{H\ell\ell} = \frac{2}{(w_Z - 4w_\ell)^2} \left[ w_\ell (w_Z - 4w_\ell) - (w_\ell - 1) (4w_\ell - w_Z) \Delta_9 \right. \\ \left. + (16w_\ell^2 - 2w_\ell (2w_Z + 5) + w_Z) \Delta_{10} - 6w_\ell (4w_\ell - w_Z - 1) C_5 \right], \quad (\text{B63})$$

and for the contribution of the new pseudoscalar  $\eta$

$$I_Z^{\eta\ell\ell} = \frac{2}{(z_Z - 4z_\ell)^2} \left[ z_\ell (z_Z - 4z_\ell) - (z_\ell - 1) (4z_\ell - z_Z) \Delta_{11} + (z_Z - 10z_\ell) \Delta_{12} \right. \\ \left. - 2z_\ell (4z_\ell - z_Z - 3) C_6 \right], \quad (\text{B64})$$

where  $\Delta_{11}$ ,  $\Delta_{12}$ , and  $C_6$  are obtained from  $\Delta_9$ ,  $\Delta_{10}$  and  $C_5$ , respectively, after the replacement  $m_H \rightarrow m_\eta$ .

As for diagram (2) of Fig. 2, it yields

$$I_Z^{\ell HV} = \frac{2\sqrt{x_\ell}}{\sqrt{x_Z} (4x_\ell - x_Z)} \left[ x_\ell (x_\ell - x_H) \Delta_{13} + (x_\ell - 1) x_\ell \Delta_{14} - 4x_\ell \Delta_{15} - 2x_Z \Delta_{16} \right. \\ \left. + 2(2x_\ell (x_H + x_Z - 1) - x_H x_Z) C_7 \right], \quad (\text{B65})$$

with

$$\Delta_{13} = B_0(0, m_H^2, m_\ell^2) - B_0(0, m_H^2, m_V^2), \quad (\text{B66})$$

$$\Delta_{14} = B_0(0, m_H^2, m_V^2) - B_0(0, m_\ell^2, m_V^2), \quad (\text{B67})$$

$$\Delta_{15} = B_0(m_\ell^2, m_H^2, m_\ell^2) - B_0(m_\ell^2, m_\ell^2, m_V^2), \quad (\text{B68})$$

$$\Delta_{16} = B_0(m_\ell^2, m_\ell^2, m_V^2) - B_0(m_Z^2, m_H^2, m_V^2), \quad (\text{B69})$$

$$C_7 = m_V^2 C_0(m_\ell^2, m_\ell^2, m_Z^2, m_H^2, m_\ell^2, m_V^2). \quad (\text{B70})$$

### 3. Anomalous magnetic dipole moment

For the loop integrals of the contributions to the AMDM of the diagrams analogue to those of Fig. 1, but with the external  $Z$  boson replaced by the photon, we have for diagram (1)

$$I_\gamma^{nVV} = -\frac{1}{8x_\ell} \left[ (x_n x_\ell (5x_\ell + 12) - 7x_n^2 x_\ell - 9x_n + 3x_n^3 - x_\ell ((x_\ell - 12)x_\ell + 17) + 6) C'_1 \right. \\ \left. + 2(x_n - 1)(x_n + x_\ell + 2) \Delta_1 + ((15 - 4x_n)x_\ell + 3(x_n + x_n^2 - 2) + x_\ell^2) \Delta'_2 \right. \\ \left. - 2x_\ell (x_n + x_\ell + 2) \right], \quad (\text{B71})$$

where the primed scalar functions  $\Delta'_i$  and  $C'_i$  are obtained from the unprimed ones by setting  $m_Z = 0$ . We note that all the three-point functions  $C'_i$  appearing in the AMDM are of the generic type  $C_0(m_A^2, m_A^2, 0, m_B^2, m_C^2, m_B^2)$ , which can be written in terms of two-point scalar functions as follows [46]

$$C_0(m_A^2, m_A^2, 0, m_B^2, m_C^2, m_B^2) = \frac{1}{\lambda(m_A^2, m_B^2, m_C^2)} \left( (m_A^2 - m_B^2 - m_C^2) \Delta_B - 2m_C^2 \Delta_C + 2(m_A^2 - m_B^2 + m_C^2) \right), \quad (\text{B72})$$

with  $\lambda(x, y, z) = (x - y - z)^2 - 4yz$  and  $\Delta_X = B_0(0, m_X^2, m_X^2) - B_0(m_A^2, m_B^2, m_C^2)$ .

As for diagram (2) we obtain a similar expression to Eq. (B54), where

$$I_{\gamma-R}^{Z'\ell\ell} = I_{\gamma-L}^{Z'\ell\ell} = -\frac{1}{4y_\ell} \left[ (3y_\ell - 1)(4y_\ell - 3)C'_2 + 2(1 - y_\ell^2)\Delta_3 + (y_\ell - 3)(2y_\ell - 1)\Delta'_4 - 2y_\ell(y_\ell + 1) \right], \quad (\text{B73})$$

and

$$I_{\gamma-LR}^{Z'\ell\ell} = -\frac{1}{2} \left[ (5 - 12y_\ell)C'_2 + 2(y_\ell - 1)\Delta_3 + (5 - 2y_\ell)\Delta'_4 + 2y_\ell \right]. \quad (\text{B74})$$

Finally, the diagram (1) of Fig 2 with the  $Z$  replaced by the photon yields the following loop functions

$$I_\gamma^{H\ell\ell} = -\frac{1}{4w_\ell} \left[ 2w_\ell + 2(w_\ell - 1)\Delta'_9 + (5 - 8w_\ell)\Delta'_{10} + 3(4w_\ell - 1)C'_5 \right], \quad (\text{B75})$$

and

$$I_\gamma^{\eta\ell\ell} = -\frac{1}{4z_\ell} \left[ 2x_\ell + 2(x_\ell - 1)\Delta'_{11} + 5\Delta'_{12} + (4x_\ell - 3)C'_6 \right]. \quad (\text{B76})$$

Again the primed scalar functions  $\Delta'_i$  and  $C'_i$  are obtained from the unprimed ones by setting  $m_Z = 0$ .

- 
- [1] T. Aoyama, M. Hayakawa, T. Kinoshita, and M. Nio, Phys. Rev. Lett. **109**, 111807 (2012), 1205.5368.
  - [2] D. Hanneke, S. Fogwell, and G. Gabrielse, Phys. Rev. Lett. **100**, 120801 (2008), 0801.1134.
  - [3] G. W. Bennett et al. (Muon g-2), Phys. Rev. **D73**, 072003 (2006), hep-ex/0602035.
  - [4] J. Kaspar (Fermilab E989), Nucl. Part. Phys. Proc. **260**, 243 (2015), 1504.01201.
  - [5] N. Saito (J-PARC g-2/EDM), AIP Conf. Proc. **1467**, 45 (2012).
  - [6] C. Patrignani et al. (Particle Data Group), Chin. Phys. **C40**, 100001 (2016).
  - [7] F. Jegerlehner and A. Nyffeler, Phys. Rept. **477**, 1 (2009), 0902.3360.
  - [8] M. Lindner, M. Platscher, and F. S. Queiroz (2016), 1610.06587.
  - [9] K. A. Olive et al. (Particle Data Group), Chin. Phys. **C38**, 090001 (2014).
  - [10] G. A. Gonzalez-Sprinberg, A. Santamaria, and J. Vidal, Nucl. Phys. **B582**, 3 (2000), hep-ph/0002203.
  - [11] A. A. Billur and M. Kksal, Phys. Rev. **D89**, 037301 (2014), 1306.5620.
  - [12] Y. Ozguven, S. C. ?nan, A. A. Billur, M. Kksal, and M. K. Bahar (2016), 1609.08348.
  - [13] M. A. Samuel, G.-w. Li, and R. Mendel, Phys. Rev. Lett. **67**, 668 (1991), [Erratum: Phys. Rev. Lett.69,995(1992)].
  - [14] S. Eidelman and M. Passera, Mod. Phys. Lett. **A22**, 159 (2007), hep-ph/0701260.
  - [15] J. Bernabeu, G. A. Gonzalez-Sprinberg, J. Papavassiliou, and J. Vidal, Nucl. Phys. **B790**, 160 (2008), 0707.2496.
  - [16] M. Fael, L. Mercolli, and M. Passera, Nucl.Phys.Proc.Suppl. **253-255**, 103 (2014), 1301.5302.
  - [17] S. Eidelman, D. Epifanov, M. Fael, L. Mercolli, and M. Passera, JHEP **03**, 140 (2016), 1601.07987.
  - [18] A. Pich, Prog. Part. Nucl. Phys. **75**, 41 (2014), 1310.7922.
  - [19] A. Heister et al. (ALEPH), Eur. Phys. J. **C30**, 291 (2003), hep-ex/0209066.
  - [20] A. Hayreter and G. Valencia, Phys.Rev. **D88**, 013015 (2013), 1305.6833.
  - [21] J. Bernabeu, G. A. Gonzalez-Sprinberg, M. Tung, and J. Vidal, Nucl. Phys. **B436**, 474 (1995), hep-ph/9411289.
  - [22] M. Schmaltz, JHEP **08**, 056 (2004), hep-ph/0407143.
  - [23] N. Arkani-Hamed, A. G. Cohen, and H. Georgi, Phys. Rev. Lett. **86**, 4757 (2001), hep-th/0104005.
  - [24] N. Arkani-Hamed, A. G. Cohen, and H. Georgi, Phys. Lett. **B513**, 232 (2001), hep-ph/0105239.
  - [25] T. Han, H. E. Logan, and L.-T. Wang, JHEP **01**, 099 (2006), hep-ph/0506313.
  - [26] F. del Aguila, J. I. Illana, and M. D. Jenkins, JHEP **03**, 080 (2011), 1101.2936.
  - [27] A. Lami, J. Portoles, and P. Roig, Phys. Rev. **D93**, 076008 (2016), 1601.07391.
  - [28] A. Lami and P. Roig, Phys. Rev. **D94**, 056001 (2016), 1603.09663.
  - [29] G. Marandella, C. Schappacher, and A. Strumia, Phys. Rev. **D72**, 035014 (2005), hep-ph/0502096.
  - [30] A. G. Dias, C. A. de S. Pires, and P. S. Rodrigues da Silva, Phys. Rev. **D77**, 055001 (2008), 0711.1154.
  - [31] J. Reuter, M. Tonini, and M. de Vries, in *Snowmass 2013: Workshop on Energy Frontier Seattle, USA, June 30-July 3, 2013* (2013), 1307.5010, URL <https://inspirehep.net/record/1243423/files/arXiv:1307.5010.pdf>.
  - [32] R. Balest et al. (CLEO), Phys. Rev. **D51**, 2053 (1995).
  - [33] G. J. van Oldenborgh and J. A. M. Vermaseren, Z. Phys. **C46**, 425 (1990).
  - [34] T. Hahn and M. Perez-Victoria, Comput. Phys. Commun. **118**, 153 (1999), hep-ph/9807565.

- [35] A. Bolaños, A. Moyotl, and G. Tavares-Velasco, Phys. Rev. **D89**, 055025 (2014), 1312.6860.
- [36] A. Moyotl and G. Tavares-Velasco, Phys. Rev. **D86**, 013014 (2012), 1210.1994.
- [37] T. Ibrahim and P. Nath, Phys. Rev. **D78**, 075013 (2008), 0806.3880.
- [38] M. Arroyo-Urena and E. Diaz, J. Phys. **G43**, 045002 (2016), 1508.05382.
- [39] J. Bernabeu, D. Comelli, L. Lavoura, and J. P. Silva, Phys. Rev. **D53**, 5222 (1996), hep-ph/9509416.
- [40] D. Gomez-Dumm and G. A. Gonzalez-Sprinberg, Eur. Phys. J. **C11**, 293 (1999), hep-ph/9905213.
- [41] W. Hollik, J. I. Illana, C. Schappacher, D. Stockinger, and S. Rigolin, Nucl.Phys. **B557**, 407 (1999), hep-ph/9808408.
- [42] W. Hollik, J. I. Illana, S. Rigolin, C. Schappacher, and D. Stockinger, Nucl.Phys. **B551**, 3 (1999), hep-ph/9812298.
- [43] G. Passarino and M. J. G. Veltman, Nucl. Phys. **B160**, 151 (1979).
- [44] R. Mertig, M. Bohm, and A. Denner, Comput. Phys. Commun. **64**, 345 (1991).
- [45] J. P. Leveille, Nucl. Phys. **B137**, 63 (1978).
- [46] G. Devaraj and R. G. Stuart, Nucl. Phys. **B519**, 483 (1998), hep-ph/9704308.